A NUMERICAL MODEL OF UNSTEADY,
SUBSONIC AEROELASTIC BEHAVIOR

BY

Thomas W. Strganac

Dissertation submitted to the Graduate Faculty of the

Virginia Polytechnic Institute and State University

in Partial Fulfillment of the Requirements for the Degree of

DOCTOR OF PHILOSOPHY

in

Engineering Mechanics

APPROVED:

_____
Dean T. Mook, Chairman

_____   _____
Daniel Frederick   Leonard Meirovitch

_____   _____
Scott L. Hendricks   William F. Hunter

August, 1987

Blacksburg, Virginia

A NUMERICAL MODEL OF UNSTEADY,
SUBSONIC AEROELASTIC BEHAVIOR

BY

Thomas W. Strganac

ABSTRACT

A method for predicting unsteady, subsonic aeroelastic responses

has been developed. The technique accounts for aerodynamic nonlinear-

ities associated with angles of attack, vortex-dominated flow, static

deformations, and unsteady behavior. The angle of attack is limited

only by the occurrence of stall or vortex bursting near the wing. The

fluid and the wing together are treated as a single dynamical system,

and the equations of motion for the structure and flowfield are inte-

grated simultaneously and interactively in the time domain. The

method employs an iterative scheme based on a predictor-corrector

technique. The aerodynamic loads are computed by the general unsteady

vortex-lattice method and are determined simultaneously with the mo-

tion of the wing. Because the unsteady vortex-lattice method predicts

the wake as part of the solution, the history of the motion is taken

into account; hysteresis is predicted. Two models are used to demon-

strate the technique: a rigid wing on an elastic support experiencing

plunge and pitch about the elastic axis, and an elastic wing rigidly

supported at the root chord experiencing spanwise bending and twist-

ing. The method can be readily extended to account for structural

nonlinearities and/or substitute aerodynamic load models. The time

domain solution coupled with the unsteady vortex-lattice method

provides the capability of graphically depicting wing and wake motion.

ACKNOWLEDGMENTS

My experience at Virginia Tech was genuinely worthwhile because
of the individuals - students, staff, and faculty - who exemplify the
university. I wish to thank the members of my graduate committee -
Professors Frederick, Meirovitch, and Hendricks - who assisted me in
my graduate program and provided an excellent educational opportunity
in the classroom. I am grateful to Mrs.   who typed
several conference papers on my behalf and became my liaison with the
university in my absence.

I am especially indebted to my mentor, Professor   , who as-
sured my education went well beyond the classroom and was not limited
by the research contained within this dissertation. His patience and
attitude was certainly tested through our collaboration. Yet I always
came away from each of our discussions with an improved understanding
of our research and an appreciation of Professor   's sincere
dedication to his profession.

I am grateful that NASA allowed me the opportunity to participate
in the Graduate Study Program. Yet, this study could not have been
realized without the continuous support of the staff of the Langley
Research Center. Individuals throughout the organization such as the
members of the Employee Development Branch, Visual and Printing
Services Branch, Computer Applications Branch, and Flight Software and
Graphics Branch have all contributed to a successful program. I am
grateful to Dr. William F. Hunter who supported my interest in this
research and served on my graduate committee. I am indebted to
Mrs.   who provided assistance in programming and

iii

graphics. And I wish to thank the members of the Technical Editing

Branch and, in particular, Miss   for the typing of

this manuscript.

Finally, I am thankful to my wife,   , who supports my

interests at her sacrifice and to our children,   and   ,

who provide the purpose.

TABLE OF CONTENTS

LIST OF FIGURES

LIST OF TABLES

NOMENCLATURE

A   wing reference area

AR   aspect ratio

{A}   generalized aerodynamic loading vector

C   nondimensional aerodynamic constant $= \rho\, \ell_c A/2\,m$

C_α nondimensional rotational damping $= c_\alpha/m\, U_\infty \ell_c$

C_m aerodynamic pitch-moment coefficient

C_n aerodynamic normal-force coefficient

C_y nondimensional translational damping $= c_y\, \ell_c/m\, U_\infty$

c   chord

c_α support rotational damping

c_y support translational damping

EI   distributed bending stiffness

F_x horizontal component of the reaction of the support structure

F_y vertical component of the reaction of the support structure

GJ   distributed torsional stiffness

g   acceleration due to gravity

I_{cg} mass moment of inertia referenced to the center of gravity

I_e mass moment of inertia referenced to the elastic axis

[I]   identity matrix

K   nondimensional inertia $= I_e/m\, \ell_c^2$

K_α nondimensional rotational stiffness $= k_\alpha/m\, U_\infty^2$

K_y nondimensional translational stiffness $= k_y\, \ell_c^2/m\, U_\infty^2$

[K]   stiffness matrix

k_α support rotational stiffness

k_y support translational stiffness

ℓ_c characteristic length = c/n

M   distributed aerodynamic pitch moment

[M]   mass matrix

M_r aerodynamic pitch moment at the reference position

M_s moment due to support structure

m   mass or distributed mass

N   distributed aerodynamic normal force

n   number of chordwise (bound) lattice elements or number of first-order equations

q   generalized coordinates

r   distance between center of gravity (cg) and elastic axis (ea), positive for cg aft of ea

{S}   static loading vector

U_∞ freestream velocity

w   displacement of the elastic axis

x_α local distance between the sectional elastic axis and center of gravity

$\bar{x}$ distance between center of gravity (cg) and the aerodynamic reference, positive for cg aft of reference

Y   nondimensional plunge degree of freedom = y/ℓ_c

α nondimensional pitch degree of freedom, or rotation about the elastic axis

η time derivative of Y or the generalized velocities (= $\dot{q}$)

ξ time derivative of α

ρ density of fluid

Φ bending or torsional free-vibration mode

ϕ static angle-of-attack

( )'   first derivative with respect to length

( )"   second derivative with respect to length

(˙)   first derivative with respect to time (or nondimensional time)

(˙˙)   second derivative with respect to time (or nondimensional time)

CHAPTER I

INTRODUCTION

1.1 General

Aeroelastic instabilities, which may be catastrophic, occur as a result of coupling between aerodynamic forces, structural forces, and mass. Therefore, the aeroelastic design of aircraft must address the structure and the aerodynamic forces within the flight environment. This concern includes the design of wings or aircraft for both flight and wind-tunnel testing.

A method to predict the aeroelastic behavior of a wing is described. The objective is to develop an improvement in aeroelastic analyses by accounting for aerodynamic nonlinearities associated with angles of attack, static deformations, vorticity-dominated flow, and unsteady behavior. This method generates a realistic simulation of aeroelastic response or instability by predicting both the motion of the wing and the motion of the fluid simultaneously. In other words, the wing and fluid are treated as a single dynamical system, and the equations of motion for the structure and flowfield are integrated simultaneously and interactively in the time domain.

The equations of motion are developed for classical two-degree-of-freedom wing motion; that is, a rigid wing which is allowed to plunge and pitch about the elastic axis. In addition, the equations of motion are developed for an elastic wing with bending and twisting. The unsteady vortex lattice method (UVLM) is used to predict the aerodynamic loads. The technique accounts for the aerodynamic nonlinearities.

A complication does exist with a time domain approach: the aerodynamic loads cannot be predicted unless the motion of the wing is known, and the motion of the wing cannot be predicted unless the aerodynamic loads are known. An iterative scheme that accounts for the interaction between the aerodynamic loads and wing motion was developed based upon a predictor-corrector approach. An advantage of the method is that it provides an excellent opportunity to animate the motions in the flowfield and wing since the governing equations are solved in the time domain.

The technique described herein provides a somewhat different approach to model flutter for a wing of arbitrary planform. The equations are developed about arbitrary static angles of attack, providing a new capability to study the associated nonlinear effects. Through the use of the UVLM one is able to treat low-aspect-ratio wings and account for the wake rollup at the wing tips. The UVLM models the wake where the history of the motion resides.

1.2 The Aeroelastic Phenomenon

Many different types of aeroelastic instabilities exist. Static instabilities include aeroelastic divergence in which the elastic restoring forces of the wing are exceeded by the aerodynamic forces. Dynamic instabilities such as flutter are caused by an exchange of energy between the aircraft and surrounding air. General aeroelastic phenomena are described by Fung (1955), Bisplinghoff, Ashley and Halfman (1955), and Dowell (1980) among others. A historical perspective of aeroelastic research is given by Collar (1978).

A complete model of the aerodynamic forces, elastic forces, and inertial forces is required to describe the unsteady aeroelastic nature of an aircraft. As Figure 1.1 depicts, this interaction among these three types of force provides the conditions necessary for potential static and dynamic instabilities. The nature of the aeroelastic problem can best be illustrated by this three-ring diagram as suggested by Yates (1971). Variations to this diagram are presented by Bisplinghoff et al. (1955), Collar (1978), and Dowell (1980).

Aerodynamic, elastic, and inertial forces are shown. The common ground between the inertial forces and elastic forces represents the free-vibration problem, the common ground between the aerodynamic forces and elastic forces represents static aeroelastic phenomena which include instabilities such as divergence, and the common ground between the aerodynamic forces and inertial forces represents dynamic stability investigations of "rigid" aircraft. The interaction of all three forces is present in the aeroelastic phenomenon known as flutter.

Flutter has been defined in many ways. Among the first to examine the nature of flutter, Theodorsen (1940) described flutter and developed a general theory which is still used today. Pines (1958) defines flutter as "a self-excited oscillatory aerodynamic instability" and states that flutter may be considered "an oscillatory instability where one degree of freedom is driven at resonance by a second degree of freedom, both at the same frequency". Hancock, Wright, and Simpson (1985) describe flutter as "a complex phenomenon where, in the classical sense of the term, two or more structural
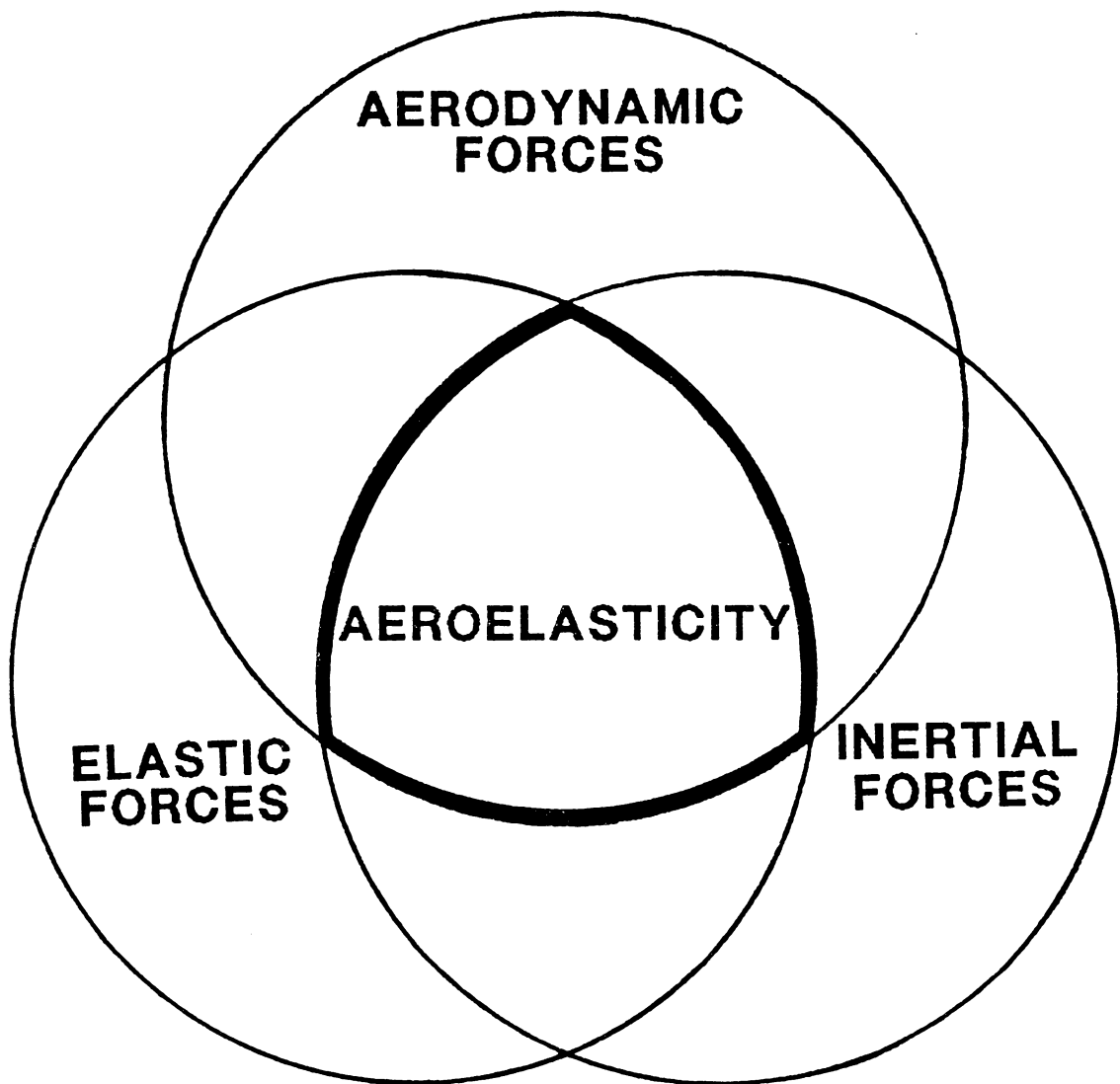
Figure 1.1. The Three-Ring Diagram.

normal modes are coupled and excited through time dependent aero-
dynamic loads". Dowell (1980) also describes the flutter phenomenon
and suggests that many types of flutter exist; these include:
"'Coalescence' or 'merging frequency' flutter", "'Single-degree-of-
freedom' flutter", and "'Divergence' or 'zero frequency' flutter".

An illustration of the flutter phenomenon is presented in Fig-
ure 1.2. A wing is initially moving through a fluid at rest. The
wing is subjected to a disturbance. In the left-hand side of the
figure the dynamic pressure is below the critical condition for flut-
ter. The bending and torsion of the wing occur at separate, unique
frequencies which are close to the natural frequencies for the free
vibration modes. The motion decays following the initial disturbance
as there is not enough energy being extracted from the freestream to
maintain the motion. In fact, the freestream is extracting energy
from the wing and damping the motion. There is aerodynamic damping
here. The system is being damped by aerodynamic effects only. In the
right-hand side of the figure the dynamic pressure is greater than the
critical pressure. Not only is the motion seen to grow in this case
but bending and torsion occur at a common frequency - a characteristic
associated with flutter. In the lower portion of the figure the shift
in system frequencies due to the dynamic pressure is illustrated. The
frequencies are the natural ones when the dynamic pressure is zero. A
coalescence occurs at a critical dynamic pressure, the system is now
in flutter.
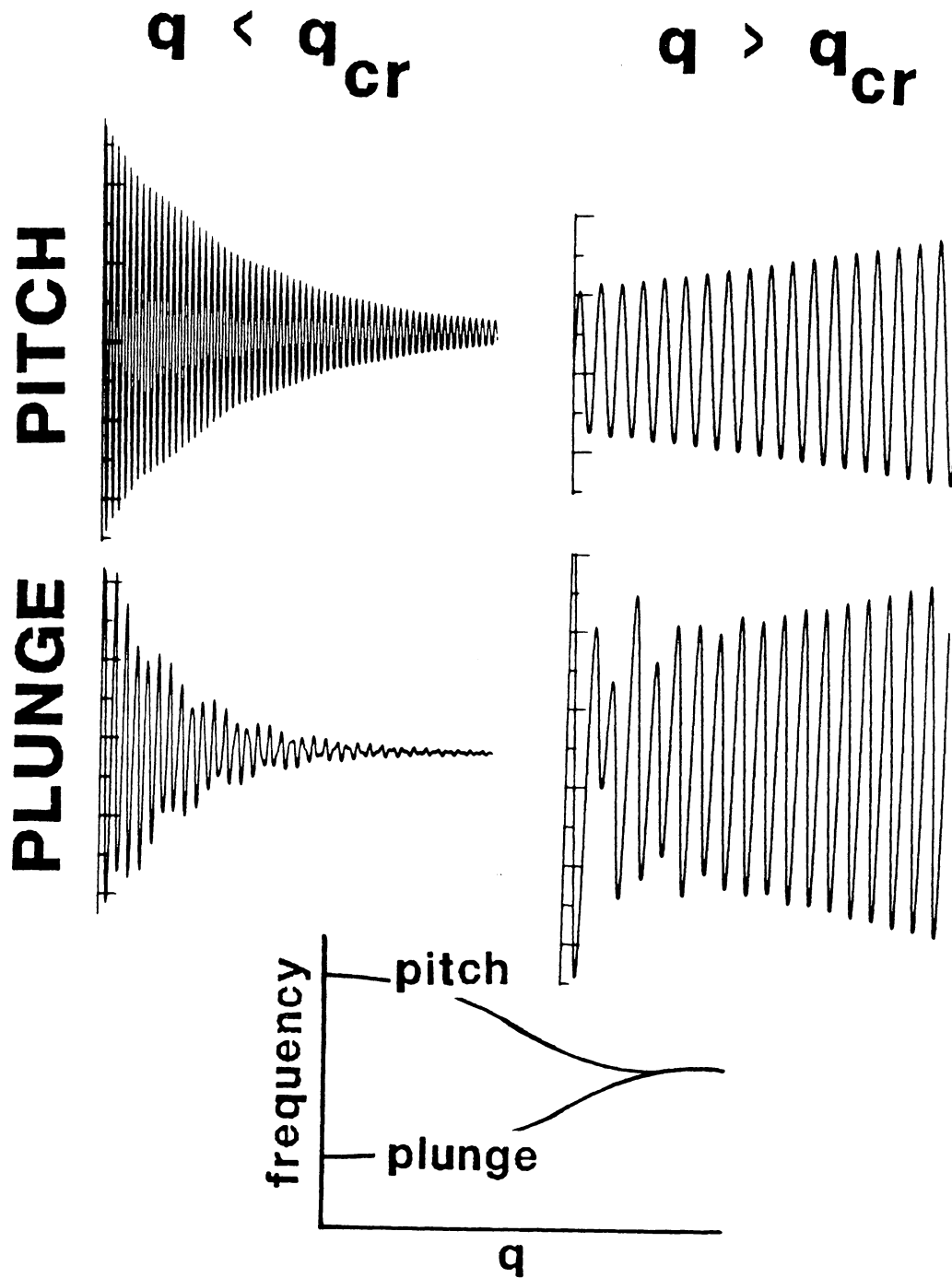
Figure 1.2. Flutter Response for a Two Degree of Freedom Example.

1.3 Literature Review

The purpose of this research is to provide an improvement in aeroelastic analysis capabilities. Through the application of the UVLM to the aeroelastic formulation new capabilities are introduced. As mentioned previously these include the modeling of aerodynamic nonlinearities and new solution strategies. These enhancements, in turn, open the door for further improvements primarily in structural nonlinearities. However, the emphasis in this research is placed on the aerodynamic model and the solution strategy; the literature review will focus on these areas.

1.3.1 Aeroelastic models

Aeroelastic research is very broad indeed. Experimental and theoretical research has been performed in structures, fluids, and dynamics as well as solution schemes associated with aeroelasticity.

Desmarais and Bennett (1978) described an approach for flutter analysis which is representative of current numerical strategies. In their method the generalized mass and mode shapes are developed through an external structural analysis package. These modes are used to describe the shape of the wing which in turn is used to compute an aerodynamic influence matrix. A subsonic kernal function approach is used to model the aerodynamics. An eigenvalue formulation is used with the governing equations. Hence, the solution is performed in the frequency domain, the governing equations are cast in a linear form, and a simple harmonic form of the solution is assumed. As we shall see, the method developed in this research is not limited by these

assumptions. The roots of this eigensolution, which are dependent

upon the velocity, density, and Mach number, are used to determine the

critical conditions necessary for flutter.

The method commonly used to determine the flutter conditions of a

wing using a frequency domain solution is illustrated in Figure 1.3.

The method, called the V-g (for Velocity-incremental damping) method,

tracks the roots of the modes used for the solution for increasing

values of velocity. A fictitious damping (the root) is determined at

each velocity which is required to satisfy the eigenvalue problem. In

the upper part of the figure we plot the roots for a 3 mode system.

The upper plane represents an unstable region; hence, when a root

enters this region the system is unstable. At only this "flutter

crossing" is the solution meaningful, yet no physical interpretation

of the motion is available. In the lower part of the figure the

frequencies for these modes are computed as the velocity increases.

Hassig (1971) and Fung (1955) described some alternate solution

schemes for the frequency domain solutions. Fung also presented many

examples, some of which will be referred to in this dissertation.

Goland and Luke (1949) outlined a method to describe the aeroelastic

character of an elastic wing.

Garrick (1969) presented several classical papers on the flutter

phenomenon, flutter determination, aerodynamic theories, and other

associated subjects. Loring (1941) introduced generalized coordinates

through the use of the natural modes to solve the flutter problem.

His work developed a systemized approach for the structural model.
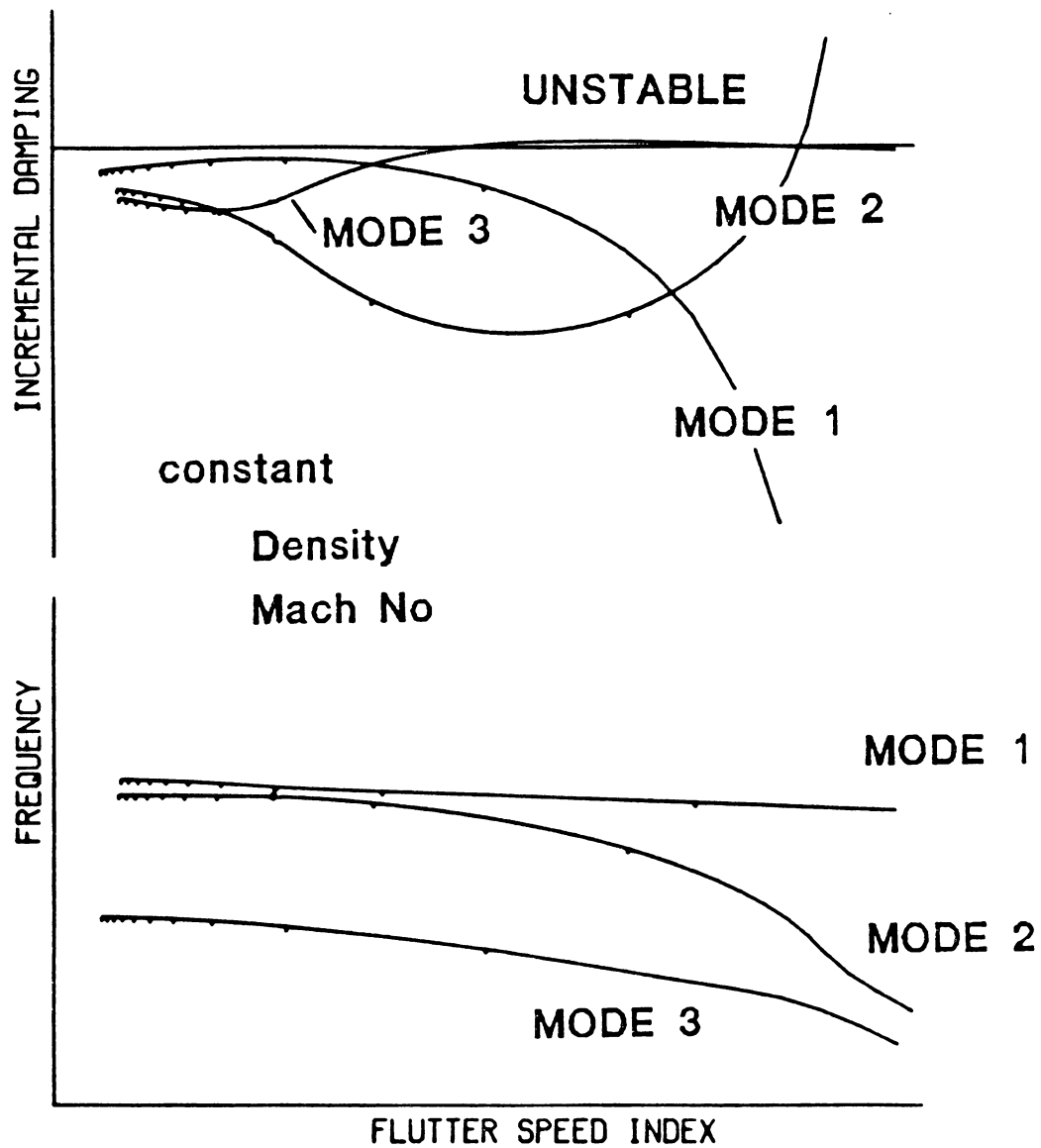
Figure 1.3. Determination of Flutter for Frequency Domain
Formulations, V-g and Frequency Diagrams.

Dowell (1980) described both frequency and time domain solutions of the aeroelastic equations. Frequency domain solutions are the most widely used since these require less resources and a more convenient solution scheme. However, a frequency domain solution does not provide a physical description of the motion as do time domain solutions. Time domain solutions, which do not assume a form of the solution (i.e. harmonic motion) as do the frequency domain schemes, provide the more general and physical approach.

A more complete formulation of the aeroelastic equations was described by Bisplinghoff (1975) and Fung (1955). Descriptions of aeroelastic phenomena were presented by Theodorsen (1940), Biot and Arnold (1948), Pines (1958), and Hancock et al. (1985). These later two papers presented physical models of flutter. Pines, in particular, examined the governing equations in a general sense and established relationships for which flutter can exist.

An aeroelastic model, which is similar in nature to the one presented in this dissertation, is described by Devers (1972). Devers developed a time domain solution of the governing equations, he too used a vortex-lattice method as an aerodynamic model. However, simplifications in his model prevented the unsteady nature of trailing edge and wing-tip vortex effects to be considered. In addition, his integration scheme assumed a form of the solution and, as a consequence, the simulation reflected this assumption.

1.3.2 Aerodynamic models

Currently, the major effort of aeroelastic research is to de-
scribe the unsteady aerodynamic loads, and, in particular, the flow in
the transonic flow regime as most recently described by Batina et al.
(1987). Edwards (1986) presented an overview of aerodynamics associ-
ated with transonic aeroelasticity.

Bisplinghoff (1975) described many different aerodynamic opera-
tors which are available for all flow regimes. Yates (1985) described
the various approaches available for aerodynamic models, which include
doublet-lattice, kernal function, velocity potential and acceleration
(pressure) potential formulations.

The research will concentrate in the subsonic regime. Theodorsen
(1940) introduced a two-dimensional functional form of the subsonic
aerodynamic operator which is still popular today. Desmarais and
Bennett (1978) implemented a subsonic kernal function indicative of
more current strategies. However, most methods are quasi-steady, lin-
ear (i.e. small angle) theories. A new approach to the subsonic aero-
dynamic model for aeroelastic analysis is introduced. The unsteady
vortex-lattice method (UVLM) provides the opportunity to address aero-
dynamic nonlinear effects associated with unsteady flow aspect ratios,
static deformations, and the angles of attack. Hence, nonlinear
aerodynamic effects may be studied as they apply to the aeroelastic
phenomenon.

Experimental investigations have demonstrated nonlinear effects.
Yates and Bennett (1971), Farmer (1982), and Yates, Wynne, and Farmer
(1982) addressed the effect angle of attack has on flutter boundaries.

Hsu (1957) addressed the effect aspect ratio has on flutter boundaries.

The development of the UVLM will be briefly reviewed. The reader is referred to the work of Kandil (1974), Maddox (1973), and most recently, Konstadinopoulos (1981) for more complete descriptions.

The unsteady vortex-lattice method, as we use it in this research, originates from the investigation of Belotserkovskiy (1966). This original work could treat arbitrary wing planforms and deformations but could not model the geometry of the wake which thereby limited it to small angles of attack. Belotserkovskiy (1968) then developed a nonlinear method to calculate the aerodynamic loads on wings with wing-tip separation in steady flows. Later, Belotserkovskiy and Nisht (1974) presented a method for the treating of rather general planforms in nonlinear unsteady flow. As part of this research, they determined the shape of the wake convecting from the wing tips and the trailing edge.

Maddox (1973) and Mook and Maddox (1974) used this vortex-lattice method and considered leading edge separation. However, this method did not account for force-free wing-tip and trailing-edge vortex sheets. Kandil (1974) and Kandil, Mook, and Nayfeh (1974) refined this approach and their results were in very good agreement with the experiments. The remarkable accuracy of vortex-lattice methods was discussed by James (1971).

Atta (1976) and Atta, Kandil, Mook, and Nayfeh (1976, 1977) extended the method to treat unsteady flows past rectangular wings with sharp-edge separation. The problem was posed in an inertial frame

which proved to be awkward. Thrasher, Mook, Kandil, and Nayfeh (1977) and Thrasher (1979) posed the problem in terms of a body-fixed frame. The approach treated rectangular wings executing arbitrary maneuvers as long as separation occurred along the wing's sharp edges and vortex bursting did not occur at or near the wing's surface.

Thrasher (1979) coupled the aerodynamic method with a predictor-corrector method to predict the flowfield, loads, and motion of a hinged rectangular wing due to a prescribed motion of a flap. This development is of particular interest since it had application to aeroelastic type problems. Kandil, Atta, and Nayfeh (1977) and Atta (1978) refined the approach to treat delta wings. Further, they developed a higher-order convection process for the wake, but this process required iteration.

Nayfeh et al. (1979) modified the method to treat small, harmonic oscillations around an arbitrary angle of attack. The general unsteady method was described by Nayfeh, Mook, and Yen (1979), Konstadinopoulos (1981) and Konstadinopoulos, Mook, and Nayfeh (1981). Most recently the general method was described by Konstadinopoulos, Thrasher, Mook, Nayfeh, and Watson (1985).

Recently, Konstadinopoulos (1984) and Konstadinopoulos, Mook, and Nayfeh (1985) developed a numerical method for simulating subsonic wing rock. More recently, Elzebda (1986) described a model for simulating two-degree-of-freedom wing rock. Elzebda, Mook, and Nayfeh (1985) described the ability of the general method to model the aerodynamics for close-coupled lifting surfaces.

1.3.3 Structural models

In this research the wing structure is represented by two differ-
ent models for demonstration purposes — a rigid wing which can pitch
and plunge about the elastic axis and an elastic wing. Currently, for
the model of the elastic wing, the elastic axis of the wing is repre-
sented by a beam which is allowed to bend and twist. No structural
nonlinearities are taken into account. The two-degree-of-freedom
model is addressed in the texts on aeroelasticity we have already
cited. Several texts (for example, see Rivello (1969)) describe the
equations of a beam which we have implemented.

The numerical model can be readily extended to include nonlinear
effects of beam flexure and torsion. Several references consider
nonlinear models, these include the work of Crespo da Silva and Hodges
(1986), Hodges and Dowell (1974), and Kaza and Kvaternik (1977).
These references address the more difficult kinematics and large
deformations associated with rotorcraft applications.

More complicated models of the wing are typically handled by fi-
nite element methods. For example, the method described by Desmarais
and Bennett (1978) implements the structural modes generated by any
experimental or analytical method. Hence, the description of struc-
tures is dependent on the capability of these alternate sources. Yet,
an advantage in the aeroelastic design of structures is gained through
the inclusion of more elaborate structural models. Ashley et al.
(1980), Bendiksen and White (1986), and Weisshaar (1987) describe the
advantages of aeroelastic tailoring of structures.

1.4 The Present Method

A method for predicting unsteady, subsonic aeroelastic responses is described. Previously, we described the application of the UVLM to the two-degree-of-freedom problem (Strganac and Mook (1986)). The introduction of the UVLM to the prediction of flutter provides the opportunity to model aerodynamic nonlinearities. Later, we extended this effort to include the elastic wing model (Strganac and Mook (1987)). Most recently, we demonstrated the simulation of flutter by animating the wing and flowfield as predicted by our model (Strganac, Mook, and Mitchum (1987)). These efforts are further described here.

In Chapter II, the equations of motion for a rigid wing on an elastic foundation are developed. Structural damping and static deflections are included. The nondimensionalization concept is also introduced.

In Chapter III, the equations of motion for an elastic wing on a fixed support are developed. The equations account for static deformations. Mass and stiffness matrices for the wing are developed. Coupling exists between bending and torsion. Structural nonlinearities are not addressed but the general formulation allows for this feature.

In Chapter IV, the unsteady vortex-lattice method is described. The computation of the wake geometry is illustrated. Comparisons of the computed pressure distribution and the sensitivity to aspect ratio are shown.

In Chapter V, the integration schemes which account for the structural dynamic and aerodynamic interaction are developed. The

methods are based upon a predictor-corrector technique, with appropriate modifications to account for aerodynamic/dynamic coupling. The convection schemes which are used to accurately generate the wake in the unsteady model are discussed. The rigid wing and elastic wing formulations are individually described as each present unique requirements.

In Chapter VI, several examples of computed results are presented. Wing response, aerodynamic loads, and pressure distributions are shown. In addition, phase planes and aerodynamic load histories are shown which further describe the physical nature of aeroelastic phenomena. Finally, the ability to take advantage of time domain solutions is graphically demonstrated. The wing and wake shape and vorticity distribution are shown at several time steps. These sequences are indicative of the animation capability which exists with the present formulation.

CHAPTER II

EQUATIONS OF MOTION FOR THE RIGID WING

2.1 Description of the System

In this chapter the equations of motion are developed for a rigid

wing on an elastic support limited to plunge and pitch about the

elastic axis. This simplified structural model, illustrated in Fig-

ure 2.1, serves as a demonstration of the technique and is described

in many references (see Fung (1955)) as a common example. However,

the equations are developed about an arbitrary static angle of attack,

ϕ, which is included in the aerodynamic model.

The wing is attached to the support by linear springs to model

stiffness characteristics and by linear dashpots to model damping

characteristics. The point of attachment is referred to as the elas-

tic axis. The center of gravity is offset from the elastic axis by

the parameter r. This offset affects sensitivity to flutter; this

effect has been described by Pines (1958) and Bisplinghoff (1975), as

well as others. The aerodynamic model accounts for spanwise effects;

hence, the aspect ratio of the wing is considered. Physical proper-

ties of the wing, stiffness (and structural damping) properties of

the support, and aerodynamic properties act on the wing section as

illustrated.
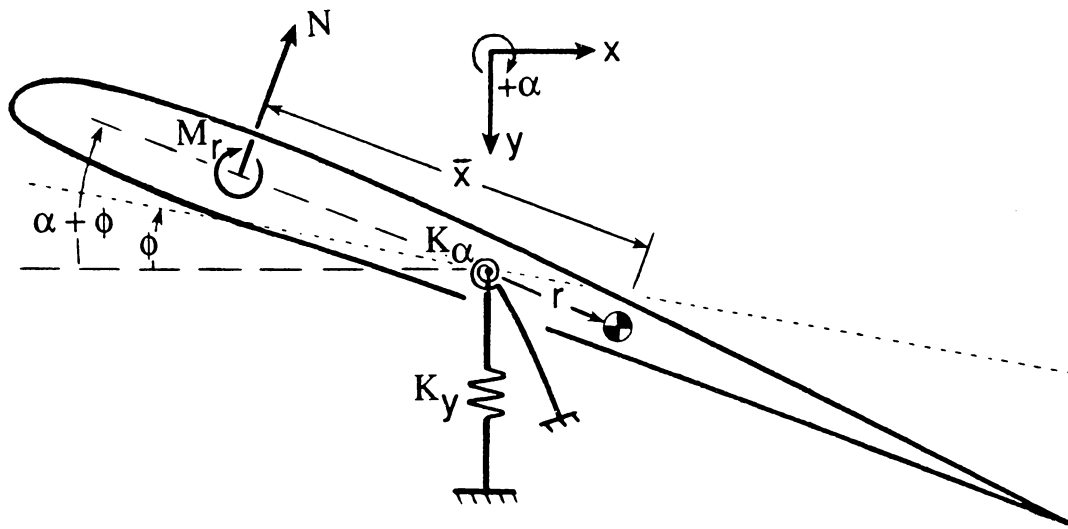
Figure 2.1. The Rigid-Wing Model.

2.2 Development of the Equations

The components of the acceleration of the center of gravity are described in the inertial frame. The x-component is expressed as

$$a_x = -r\ddot{\alpha} \sin(\alpha + \phi) - r\dot{\alpha}^2 \cos(\alpha + \phi) \qquad (2.1)$$

and the y-component is expressed as

$$a_y = \ddot{y} + r\ddot{\alpha} \cos(\alpha + \phi) - r\dot{\alpha}^2 \sin(\alpha + \phi) \qquad (2.2)$$

where α and y are the coordinates which describe the pitch and punge motion. The location of the center of gravity relative to the elastic axis is given by r, which is a positive quantity if the center of gravity is aft (i.e., towards the trailing edge) of the elastic axis.

Summing forces in the X direction results in the following equation:

$$F_x + N \sin(\alpha + \phi)$$

$$= m\{-\ddot{\alpha}r \sin(\alpha + \phi) - \dot{\alpha}^2 r \cos(\alpha + \phi)\} \qquad (2.3)$$

Summing forces in the Y direction results in the following equation:

$$F_y - N \cos(\alpha + \phi)$$

$$= m\{\ddot{y} + \ddot{\alpha}r \cos(\alpha + \phi) - \dot{\alpha}^2 r \sin(\alpha + \phi)\} \qquad (2.4)$$

Summing moments about the wing's center of gravity results in the following equation:

$$M_r + M_s + N\bar{x} - rF_y \cos(\alpha + \phi)$$

$$+ r \sin(\alpha + \phi)F_x = I_{cg}\ddot{\alpha} \qquad (2.5)$$

where $\bar{x}$ is the distance between the reference position of the aerodynamic loads and the mass center of the wing and is a positive quantity if the mass center is aft of the reference position. The reactions of the springs and dashpots are denoted by F_x, F_y, and M_s. Equations (2.3) and (2.4) are substituted into Equation (2.5), and the result is the following differential equation:

$$I_{cg}\ddot{\alpha} = N\bar{x} + M_r + M_s - rN - mr\ddot{y} \cos(\alpha + \phi) - r^2 m\ddot{\alpha} \qquad (2.6)$$

Equations (2.4) and (2.6) represent the differential equations which describe the motion of the system. Linear elastic spring and damping forces and moments are defined as follows:

$$F_y = -c_y\dot{y} - k_y y$$

$$M_s = -c_\alpha\dot{\alpha} - k_\alpha\alpha$$

These expressions are substituted into Equations (2.4) and (2.6). Structural nonlinearities could be introduced in the spring and damping model.

The force and moment equations are now rewritten as

$$m\ddot{y} + mr\ddot{\alpha} \cos(\alpha + \phi) - m\dot{\alpha}^2 r \sin(\alpha + \phi)$$

$$= -N \cos(\alpha + \phi) - k_y y - C_y \dot{y} \qquad (2.7)$$

$$I_{cg}\ddot{\alpha} + r^2 m\ddot{\alpha} + rm\ddot{y} \cos(\alpha + \phi)$$

$$= N\bar{x} - c_\alpha \dot{\alpha} - k_\alpha \alpha + M_r - rN - r^2 m\ddot{\alpha} \qquad (2.8)$$

The form of these equations can be simplified by introducing the following:

$$I_e = I_{cg} + r^2 m$$

and

$$M = M_r + (\bar{x} - r)N$$

Equations (2.7) and (2.8) are now rewritten as

$$I_e\ddot{\alpha} + mr\ddot{y} \cos(\alpha + \phi) + k_\alpha \alpha + c_\alpha \dot{\alpha} = M \qquad (2.9)$$

and

$$m\ddot{y} + mr\ddot{\alpha} \cos(\alpha + \phi) - mr\dot{\alpha}^2 \sin(\alpha + \phi)$$

$$+ k_y y + c_y \dot{y} = -N \cos(\alpha + \phi) \qquad (2.10)$$

The linear form of Equations (2.9) and (2.10) agrees with the equations derived by Fung (1955).

The numerical integration scheme which is described in Chapter V requires first-order differential equations. To this end, Equations (2.9) and (2.10) are solved simultaneously to provide equations in terms of the second-order time derivatives. These equations are:

$$
\ddot{y} = \left[\frac{1}{I_e - mr^2 \cos^2(\alpha + \phi)} \right] \left\{ (k_\alpha \alpha + c_\alpha \dot{\alpha}) r \cos(\alpha + \phi) \right.
$$

$$
+ I_e \dot{\alpha}^2 r \sin(\alpha + \phi) - \frac{I_e}{m} (k_y y + c_y \dot{y})
$$

$$
\left. - Mr \cos(\alpha + \phi) - \frac{NI_e \cos(\alpha + \phi)}{m} \right\} \qquad (2.11)
$$

$$
\ddot{\alpha} = \left[\frac{1}{I_e - mr^2 \cos^2(\alpha + \phi)} \right] \left\{ -c_\alpha \dot{\alpha} - k_\alpha \alpha + M \right.
$$

$$
- r^2 \dot{\alpha}^2 m \sin(\alpha + \phi) \cos(\alpha + \phi)
$$

$$
\left. + r \cos(\alpha + \phi)(k_y y + c_y \dot{y}) + Nr \cos^2(\alpha + \phi) \right\} \qquad (2.12)
$$

where the aerodynamic normal force, N, and pitch moment, M, are defined as

$$
N = \frac{1}{2} \rho U_\infty^2 A C_n \qquad (2.13)
$$

$$
M = \frac{1}{2} \rho U_\infty^2 A n \ell_c C_m \qquad (2.14)
$$

M is referenced to the elastic axis. The quantity $n\ell_c$ is the full chord of the wing.

2.3 Nondimensionalized Form of the Governing Equations

The governing equations of the UVLM have been written in a non-dimensional form through the introduction of the characteristic length, ℓ_c, characteristic velocity, U_∞, and the resulting characteristic time, $(\tau = \ell_c/U_\infty)$. Equation (2.11) is also rendered non-dimensional by dividing both sides of the equation by U_∞^2/ℓ_c. This equation is now expressed as

$$\ddot{Y} = \frac{1}{K - r^2 \cos^2(\alpha + \phi)} \left[(K_\alpha \alpha + C_\alpha \dot{\alpha} - nCC_m)r \cos(\alpha + \phi) \right.$$

$$\left. + K\{\dot{\alpha}^2 r \sin(\alpha + \phi) - K_y Y - C_y \dot{Y} - CC_n \cos(\alpha + \phi)\} \right] \qquad (2.15)$$

where $K = I_e/m\ell_c^2$ is introduced as a nondimensional inertia and $C = \rho\ell_c A/2m$ is introduced as a nondimensional aerodynamic constant. Hence, we also utilize the mass, m, to characterize the physical properties in nondimensional form. Other terms in Equation (2.15) have been rearranged and represent the necessary collection of terms for the nondimensional form. All quantities are nondimensional.

Similarly, Equation (2.12) is nondimensionalized by dividing both sides of the equation by U_∞^2/ℓ_c^2. This equation is now expressed as

$$\ddot{\alpha} = \frac{1}{K - r^2 \cos^2(\alpha + \phi)} \{ (C_y \dot{Y} + K_y Y)r \cos(\alpha + \phi)$$

$$- r^2 \dot{\alpha}^2 \sin(\alpha + \phi) \cos(\alpha + \phi) - (C_\alpha \dot{\alpha} + K_\alpha \alpha)$$

$$+ C(n C_m + r \cos^2(\alpha + \phi)C_n) \} \qquad (2.16)$$

One should note that the velocity now appears only in the spring and damping terms. K_α and K_y contain the square of the speed in the denominator. C_α and C_y contain the speed in the denominator. Hence, the effective stiffness and damping of the system decreases as the freestream speed increases.

CHAPTER III

EQUATIONS OF MOTION FOR THE ELASTIC WING

3.1 Description of the System

In this chapter the equations of motion for an elastic wing are developed by using an energy approach. This wing is illustrated in Figure 3.1. Small displacements about an equilibrium position are assumed. The angle of attack is introduced into the equations. The wing is allowed to bend and twist about an elastic axis not necessarily coincident with the inertial axis. Thus, there is inertial as well as aerodynamic coupling between wing bending and torsion.

The wing is represented as a cantilevered beam, which can both bend and twist. The cross section of the beam is assumed to be rigid. The wing root is rigidly fixed. The physical properties may vary along the span of the wing. Spanwise variation in the aerodynamic loading is considered. The solution of the governing equations consists of static and dynamic contributions. The statically deformed shape due to steady aerodynamic loads and the distributed weight is determined. Franz, Krenz, and Kotschote (1984) discussed the importance of deformations due to static loads on aerospace vehicles, particularly wind-tunnel models.

3.2 Development of the Equations

We ignore the out-of-plane (that is, the spanwise) motion. The components of the velocity are expressed as

$$v_x = -x_\alpha(y) \sin(\alpha(y,t)) \, \dot{\alpha}(y,t) \qquad (3.1)$$
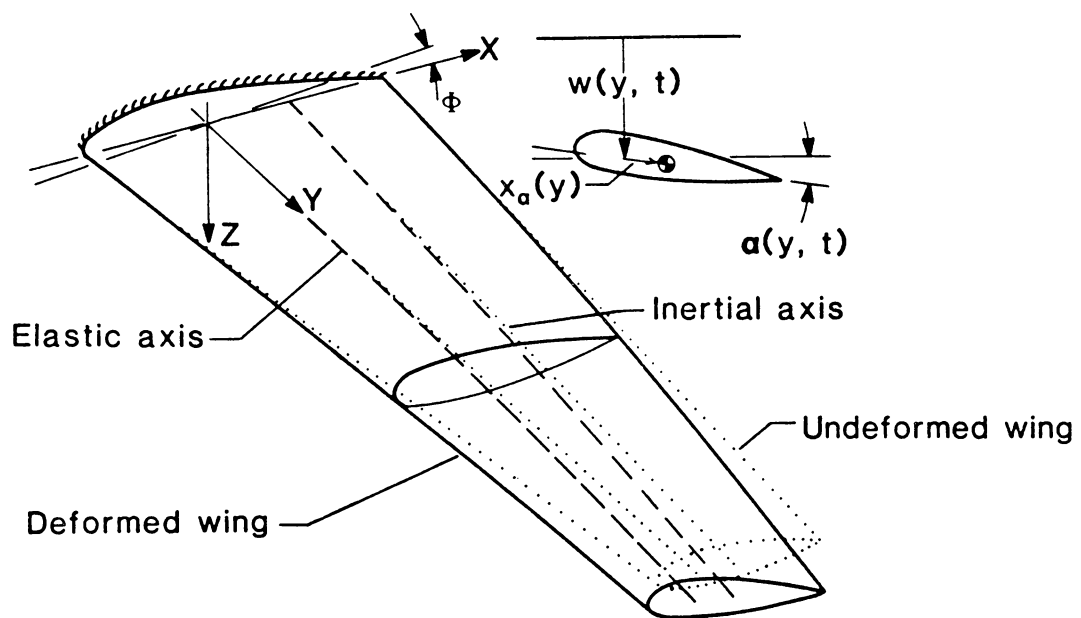
Figure 3.1. The Elastic-Wing Model.

$$v_z = \dot{w}(y,t) + x_\alpha(y) \cos(\alpha(y,t)) \, \dot{\alpha}(y,t) \qquad (3.2)$$

The kinetic energy of the system is expressed as

$$T = \int_0^L \frac{1}{2} \left[m(y)(\{\dot{w} + x_\alpha(y)(\cos \alpha)\dot{\alpha}\}^2 \right.$$

$$\left. + \{x_\alpha(y)(\sin \alpha)\dot{\alpha}\}^2) + I_{cg}(y)\dot{\alpha}^2 \right] dy \qquad (3.3)$$

The potential energy of the system is expressed as

$$V = \int_0^L \frac{1}{2} \left\{ EI(y)w''^2 + GJ(y)\alpha'^2 - m(y)g(w + x_\alpha(y) \sin \alpha) \right\} dy \quad (3.4)$$

The distributed aerodynamic loads are provided by the unsteady vortex-lattice method (UVLM). The work done by the aerodynamic loading is expressed as

$$W = \int_0^L \{-Nw(y,t) + M\alpha(y,t)\} \, dy \qquad (3.5)$$

This aerodynamic spanwise loading is dependent upon the motion, and the motion, in turn, is dependent upon the aerodynamic loads. The normal force and pitching moment are functions which should be expressed as

$$N = [w, \dot{w}, w', \alpha, \dot{\alpha}, t; \phi, AR, \text{planform}]$$

$$M = [w, \dot{w}, w', \alpha, \dot{\alpha}, t; \phi, AR, \text{planform}]$$

According to Hamilton's principle,

$$\int_0^t \int_0^L (\delta T - \delta V + \delta W) \, dy \, dt = 0 \tag{3.6}$$

Substituting T, V, and W into Equation (3.6), one obtains the following differential equations:

$$m\ddot{w} + mx_\alpha \cos(\alpha)\ddot{\alpha} - mx_\alpha \sin(\alpha)\dot{\alpha}^2$$

$$+ (EI \, w'')'' - mg = -N \tag{3.7}$$

$$I_e\ddot{\alpha} + mx_\alpha \cos(\alpha)\ddot{w} - (GJ \, \alpha')' - mgx_\alpha \cos(\alpha) = M \tag{3.8}$$

The linear form of these equations is

$$m\ddot{w} + mx_\alpha\ddot{\alpha} + (EI \, w'')'' - mg = -N \tag{3.9}$$

$$I_e\ddot{\alpha} + mx_\alpha\ddot{w} - (GJ \, \alpha')' - mgx_\alpha = M \tag{3.10}$$

where all properties vary along the length.

For the case where Equations (3.9) and (3.10) represent a cantilevered wing, the boundary conditions for these equations are

$$w(0,t) = w'(0,t) = w''(L,t) = (EI(L)w''(L,t))' = 0$$

and $\tag{3.11}$

$$\alpha(0,t) = \alpha'(L,t) = 0$$

3.3 Static and Dynamic Equations

The solution of Equations (3.9) and (3.10) provides both the static and dynamic contributions. The developed equations will yield the static solution for cases of decaying motion. However, the solution may require unnecessary computations for static solutions only; therefore, $w(y,t)$ and $\alpha(y,t)$ are redefined as

$$w(y,t) = w_s(y) + w_d(y,t) \tag{3.12}$$

and

$$\alpha(y,t) = \alpha_s(y) + \alpha_d(y,t) \tag{3.13}$$

where the subscripts s and d refer to the static and dynamic solutions. Now these equations become

$$m\ddot{w}_d + mx_\alpha \ddot{\alpha}_d + (EIw_d'')'' + (EIw_s'')'' - mg = -N \tag{3.14}$$

and

$$I_e \ddot{\alpha}_d + mx_\alpha \ddot{w}_d - (GJ\alpha_s')' - (GJ\alpha_d')' - mgx_\alpha = M \tag{3.15}$$

From Equations (3.14) and (3.15), the equations for the static deformations and the dynamical equations for small motion about the static deformations are

$$(EIw_s'')'' - mg = -N_s \tag{3.16}$$

$$-(GJ\alpha_s')' - mgx_\alpha = M_s \tag{3.17}$$

$$m\ddot{w}_d + mx_\alpha \ddot{\alpha}_d + (EIw_d'')'' = -N_d \tag{3.18}$$

$$I_e \ddot{\alpha}_d + m x_\alpha \ddot{w}_d - (GJ\alpha_d')' = M_d \qquad (3.19)$$

Meirovitch (1980) describes a method of solution to these equations by an expansion of the dependent variables. The variables w and α are represented by expansions in terms of the natural free vibration modes of the system.

$$w = \sum_{i=1}^{I} q_i \, \Phi_i \qquad (3.20)$$

and

$$\alpha = \sum_{j=I+1}^{J} q_j \, \Phi_j \qquad (3.21)$$

where the q_i and q_j are the generalized coefficients and the Φ_i and Φ_j are the modes chosen as the comparison functions, and where

I = number of bending modes selected,

J − I = number of torsion modes selected, and

J = total number of modes selected to represent the solution.

3.3.1 Equations governing the static contribution

These expansions are substituted into the static Equations (3.16) and (3.17). The result becomes

$$\sum_{i=i}^{I} (EI\Phi_i'')'' \, q_i - mg = -N_s \qquad (3.22)$$

$$-\sum_{j=I+1}^{J} (GJ\Phi_j')' \, q_j = M_s + mgx_\alpha \qquad (3.23)$$

Multiplying the first equation by Φ_r for $r=1,2,\ldots,I$ and then integrating along the span, one obtains

$$\int_0^L \sum_{i=1}^I (EI\Phi_i'')''\Phi_r \; dy \; q_i - \int_0^L mg\Phi_r \; dy = -\int N_s \Phi_r \; dy \qquad (3.24)$$

Multiplying the second equation by Φ_s for $S=I+1,\ldots,J$ and then integrating along the span, one obtains

$$-\int_0^L \sum_{j=I+1}^J (GJ\Phi_j')'\Phi_s \; dy \; q_j$$

$$= \int_0^L M_s \Phi_s \; dy + \int_0^L mgx_\alpha \Phi_s \; dy \qquad (3.25)$$

In Equations (3.24) and (3.25), the first term is integrated by parts and the boundary conditions, Equation (3.11), are imposed. With rearrangement these equations are rewritten as

$$\sum_{i=1}^I \int_0^L EI\Phi_i''\Phi_r'' \; dy \; q_i = \int_0^L mg\Phi_r \; dy - \int_0^L N_s \Phi_r \; dy \qquad (3.26)$$

and

$$\sum_{j=I+1}^J \int_0^L GJ\Phi_j'\Phi_s' \; dy \; q_j = \int_0^L M_s \Phi_s \; dy + \int_0^L mgx_\alpha \Phi_s \; dy \qquad (3.27)$$

The above expressions represent J equations, which in matrix form may be written as

$$[K]\{q\}_s = [\{A_s\} + \{S\}] \qquad (3.28)$$

The stiffness matrix [K] is partitioned as

$$
\begin{bmatrix} K_{11} & K_{12} \\ K_{12} & K_{22} \end{bmatrix}
$$

where

$$
K_{11} = \int_0^L EI\Phi_i''\Phi_j'' \, dy
\qquad\qquad
\begin{array}{l} \text{for } i = 1,2,\ldots,I \\ j = 1,2,\ldots,I \end{array}
$$

$$
K_{12} = K_{21} = 0
$$

$$
K_{22} = \int_0^L GJ\Phi_i'\Phi_j' \, dy
\qquad\qquad
\begin{array}{l} \text{for } i = I+1,\ldots,J \\ j = I+1,\ldots,J \end{array}
$$

$\{A_s\}$ is the static aerodynamic loading vector and is defined as

$$
\{A_s\} = \left\{ \begin{array}{c} \int_0^L - N_s\Phi_i \, dy \\ \vdots \\ \int_0^L M_s\Phi_j \, dy \end{array} \right\}
\qquad\qquad
\begin{array}{l} \text{for } i=1,2,\ldots,I \\ j=I+1,\ldots,J \end{array}
$$

$\{S\}$ is the static loading (due to weight) vector and is defined

as

$$
\{S\} = \left\{ \begin{array}{c} \int_0^L mg\Phi_i \, dy \\ \vdots \\ \int_0^L mgx_\alpha \, \Phi_j \, dy \end{array} \right\}
\qquad\qquad
\begin{array}{l} \text{for } i=1,2,\ldots,I \\ j=I+1,\ldots,J \end{array}
$$

3.3.2 Equations governing the dynamic contribution

We now concentrate on the dynamic equations. Substituting the series representation into the governing equations ((3.18) and (3.19)) for the dynamic solution yields the following equations:

$$\sum_{i=1}^{I} m\ddot{q}_i \Phi_i + \sum_{j=I+1}^{J} mx_\alpha \ddot{q}_j \Phi_j + \sum_{i=1}^{I} q_i (EI\Phi_i'')'' = -N_d \qquad (3.29)$$

$$\sum_{i=1}^{I} mx_\alpha \ddot{q}_i \Phi_i + \sum_{j=I+1}^{J} I_e \ddot{q}_j \Phi_j - \sum_{j=I+1}^{J} q_j (GJ\Phi_j')' = M_d \qquad (3.30)$$

Multiplying the first equation by Φ_r for $r = 1,2,\ldots,I$ and integrating along the span we obtain the following expression:

$$\sum_{i=1}^{I} \ddot{q}_i \int_0^L m\Phi_i \Phi_r \, dy + \sum_{j=I+1}^{J} \ddot{q}_j \int_0^L mx_\alpha \Phi_j \Phi_r \, dy$$

$$+ \sum_{i=1}^{I} q_i \int_0^L EI\Phi_i'' \Phi_r'' \, dy = -\int_0^L N_d \Phi_r \, dy \qquad (3.31)$$

Multiplying the second equation by Φ_s for $s = R+1,\ldots J$ and integrating along the span we obtain the following expression:

$$\sum_{i=1}^{I} \ddot{q}_i \int_0^L mx_\alpha \Phi_i \Phi_s \, dy + \sum_{j+I+1}^{J} \ddot{q}_j \int_0^L I_e \Phi_j \Phi_s \, dy$$

$$+ \sum_{j=I+1}^{J} q_j \int_0^L GJ\Phi_j' \Phi_s' \, dy = \int_0^L M_d \Phi_s \, dy \qquad (3.32)$$

The third term in each of these expressions has been integrated by parts and the boundary conditions, Equation (3.11), are imposed. The result is a more simplified form of the equations. The above expressions represent a number of equations (J) equal to the total number of modes chosen to represent the system. These equations may be written in the following matrix form:

$$[M]\{\ddot{q}\} + [K]\{q\} = \{A_d\} \qquad\qquad (3.33)$$

The mass matrix [M] is partitioned as

$$[M] = \begin{bmatrix} M_{11} & M_{12} \\ M_{21} & M_{22} \end{bmatrix}$$

where the terms in [M] are defined as follows:

$$M_{11} = \int_0^L m\Phi_i\Phi_j \, dy \qquad\qquad \text{for } i = 1,2,\dots,I \\ j = 1,2,\dots,I$$

$$M_{12} = M_{21} = \int_0^L mx_\alpha \, \Phi_i\Phi_j \, dy \qquad\qquad \text{for } i = 1,2,\dots,I \\ j = I+1,\dots,J$$

$$M_{22} = \int_0^L I_e\Phi_i\Phi_j \, dy \qquad\qquad \text{for } i = I+1,\dots,J \\ j = I+1,\dots,J$$

The stiffness matrix [K] is as previously defined.

The right-hand side contains the aerodynamic contribution and is expressed as follows:

$$\{A_d\} = \left\{ \begin{array}{c} \int\limits_0^L -N_d \Phi_i \ dy \\ \vdots \\ \int\limits_0^L M_d \Phi_j \ dy \end{array} \right\} \qquad\qquad \begin{array}{l} \text{for } i = 1,2,\ldots,I \\ j = I+1,\ldots,J \end{array}$$

N_d and M_d represent the sectional normal force and moment referenced at the elastic axis and computed from the dynamic solutions.

$[M]$ and $[K]$ are symmetric. In addition, these equations may be inertially uncoupled if the sectional center of gravity and elastic axis are coincident such that $x_\alpha = 0$. However, the equations are still coupled through the aerodynamic loads.

The equations are to be cast in a manner similar to that of the two-degree-of-freedom formulation. Therefore, $\eta = \dot{q}$ is introduced which allows the governing equations to be written in state space form.

$$\left\{ \begin{array}{c} \{\dot{\eta}\} \\ \{\dot{q}\}_d \end{array} \right\} = \left[\begin{array}{cc} 0 & -[M]^{-1}[K] \\ [I] & 0 \end{array} \right] \left\{ \begin{array}{c} \{\eta\} \\ \{q\}_d \end{array} \right\} + \left\{ \begin{array}{c} [M]^{-1} \{A\}_d \\ 0 \end{array} \right\} \qquad (3.34)$$

The above expressions provide a set of first-order differential equations, the solution of which describes the motion of the elastic wing. The integration scheme of these equations will be described subsequentially.

CHAPTER IV

AERODYNAMIC LOADS, THE UNSTEADY VORTEX-LATTICE METHOD

4.1 Overview

The equations of motion and the associated integration scheme are formulated in a manner which permit the aerodynamic loads to be determined concurrently with the motion. In this chapter, a technique is described which models the aerodynamic loads using the unsteady vortex lattice method (UVLM). This method has been completely described by Konstadinopoulos (1981); hence, the technique as applied in this research will be briefly reviewed.

The UVLM is a numerical model of the three-dimensional flowfield, which can be used to treat arbitrary maneuvers of wings of arbitrary planforms, including highly swept delta wings which exhibit leading edge separation, multiple closely coupled lifting surfaces, and low-aspect-ratio planforms. It can also treat arbitrary angles of attack and camber as long as stall or vortex bursting in the near wake does not occur. The method accounts for the nonlinear effects of the wakes adjoining the tips and trailing edge.

The ability of the UVLM to predict accurate spanwise distribution of loads has been demonstrated. In addition to the work of Konstadinopoulous, it is also worth mentioning other applications of the UVLM. The method was used to model aerodynamics of close-coupled lifting surfaces (Elzebda (1986)). Mook and Nayfeh (1985) demonstrated the method for high-angle-of-attack aerodynamics. Kobayakawa and Onuma (1985) applied the vortex-lattice method to model propeller

aerodynamics. Thomas and Nerney (1976) implemented the vortex-lattice method (coupled with slender body theory) to predict the aerodynamics of wing-body combinations. Kandil, Mook, and Nayfeh (1976) applied the UVLM to aircraft interference problems.

The approach assumes that the flow is incompressible and inviscid and does not separate on the wing, but that separation occurs along the sharp edges where the Kutta Condition is imposed in a steady flow. At each time step this vorticity, which forms the wake, is convected at the local particle velocity; thus, the position of and the distribution of vorticity in the wake are part of the solution. The wake contains the history of the flow. Consequently, the velocity induced by it at the present time reflects the previous motion.

In the aerodynamic model the vorticity in the flow is restricted to a thin region around the lifting surface and its wake. The flow outside this region is considered irrotational. The wing and wake are modeled as a sheet of vorticity. The wing portion, commonly referred to as the bound-vortex sheet, is specified, and as a result, a finite pressure jump exists across it. The wake portion, commonly referred to as the free-vortex sheet, is not specified but rather is force-free and is formed as part of the solution in such a way that no pressure jump exists across the wake.

4.2 A Description of the Method

4.2.1 The wing representation

The vortex-lattice representation of a typical wing is illustrated in Figure 4.1. The wing is modeled by a lattice of discrete
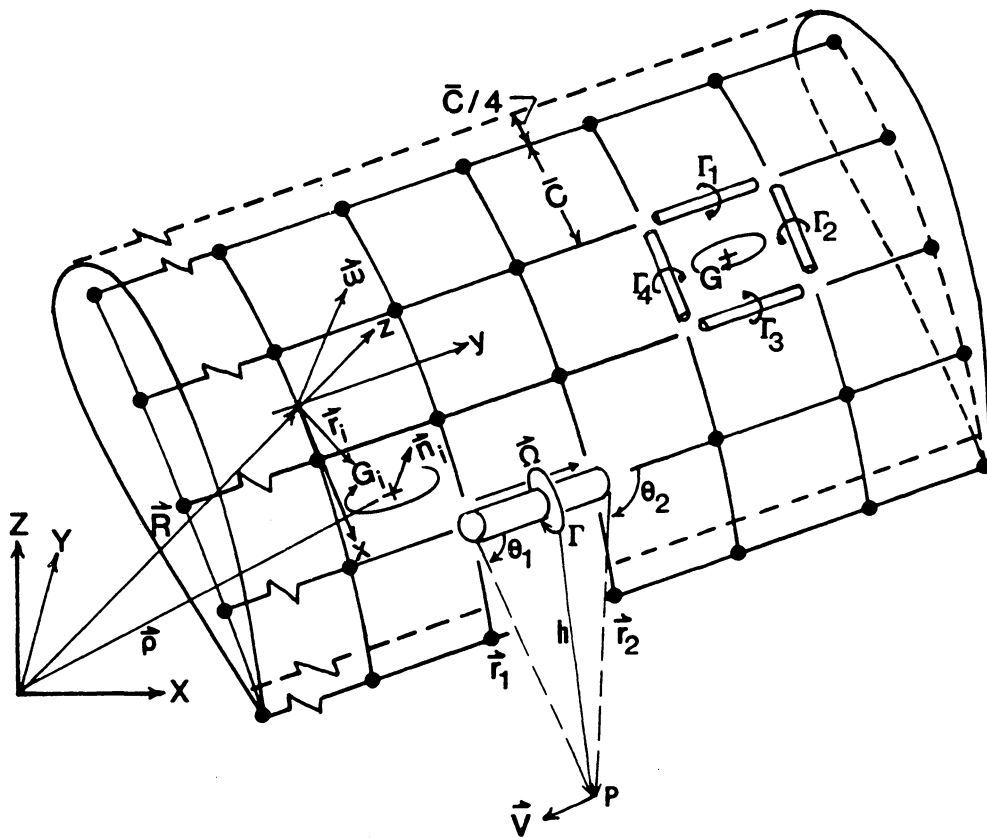
Figure 4.1. The Unsteady Vortex-Lattice Method.

vortex filaments. Each element of area on the wing is surrounded by a closed loop of constant-circulation vortex segments. These segments join at the nodes, where the loops make sharp (typically 90°) turns. A node is the intersection of the segments and is represented by a heavy dot in the figure. Control points are located at the center of each element; two typical control points are shown in the figure (denoted by small crosses).

The individual discrete vortex segments connecting the nodes are typically members of two different loops (the exceptions are the segments along the edges). Consequently, the circulation around an individual segment is the algebraic sum of the circulations around the two loops to which it belongs. In Figure 4.1 the Γ's represent circulations around the individual segments, and the G's represent circulations around the closed loops of segments. For example, referring to the figure, Γ_1 is $G_9 - G_4$.

4.2.2 Kinematic considerations

Two coordinate systems are defined: the fixed inertial frame and a moving frame fixed to the wing and aligned with the wing root and elastic axis. This would be a deforming coordinate system for the elastic-wing model. The problem is posed in terms of the moving reference frame. As described in the chapters addressing the equations of motion, the dynamic model will be posed in terms of a translating, but nonrotating, coordinate system.

The position of a point may be described as

$$\vec{\rho} = \vec{R} + \vec{r} \tag{4.1}$$

The velocity of this point is given by

$$\dot{\vec{\rho}} = \dot{\vec{R}} + \vec{v} + \vec{\omega} \times \vec{r} \qquad (4.2)$$

where $\vec{v}$ is the velocity vector relative to the moving frame and $\vec{\omega}$ is the angular velocity of the moving frame. The components of the velocity vectors are expressed in terms of the moving frame. The components of the angular velocity in the moving frame may be expressed in terms of the derivatives of the Euler angles. A complete description of the coordinate transformations and Euler angles for general motion is presented in Konstadinopoulos's work. The transformations required for this research involve only the pitch angle. These transformations are described in the chapter which presents the development of the governing equation of motions.

4.2.3 The Biot-Savart Law

The equation that serves as the foundation of the UVLM is the Biot-Savart Law (see Karamcheti (1980)) which gives the velocity induced at point P (see Fig. 4.1) by an individual vortex segment.

$$\vec{v} = \frac{\Gamma}{4\pi h} (\cos \theta_1 - \cos \theta_2) \frac{\vec{\Omega} \times \vec{r}_1}{\left| \vec{\Omega} \times \vec{r}_1 \right|} \qquad (4.3)$$

The graphical representation of this equation is illustrated in Figure 4.1. Γ represents the circulation associated with a vortex filament described by $\vec{\Omega}$ and h is the perpendicular distance from the filament to the point P.

Equation (4.3) is used to establish the aerodynamic influence matrix and the local velocity at a point as affected by all bound and free vortex filaments. The velocity field generated identically satisfies the continuity equation by this equation. The continuity equation for an incompressible fluid is

$$\vec{\nabla} \cdot \vec{V} = 0 \tag{4.4}$$

4.2.4 The boundary conditions

The flow must satisfy the following boundary conditions. The disturbance velocity must approach zero far away from the lifting surface and wake (satisfied identically through the Biot-Savart Law), and the relative velocity normal to the lifting surface must vanish on the lifting surface,

$$\left(\vec{V} - \vec{V}_{1s}\right) \cdot \vec{n} = 0 \text{ on the wing} \tag{4.5}$$

where V_{1s} is the velocity of the lifting surface and $\vec{n}$ is the normal to the lifting surface. In addition, for an inviscid fluid the Kelvin-Helmholtz theorem, which requires that all vorticity be transported with the fluid particles when the pressure is continuous, is used to obtain the position of the force-free wake. This theorem may be stated as

$$\frac{D\Gamma}{Dt} = 0 \tag{4.6}$$

where Γ is the circulation around any arbitrary closed loop.

The vortex sheet representing the wing is approximated by a lattice. Thus, the no-penetration condition, Equation (4.5), is enforced at only a finite number of points, the control points of the bound lattice. These control points are located at the centroids of the elements, and the normal vectors are obtained by forming the cross product of the diagonals in each element.

This lattice serves as a computationally expedient imitation of the boundary layers on the lifting surface and the free-shear layers in the wake. The velocity field induced by the vorticity is computed according to the Biot-Savart law; consequently, the velocity field satisfies the continuity equation and decays far from the wing and its wake.

4.2.5 The calculation of the circulation

The circulations of the loops, the G_i in Figure 4.1, are obtained from the no-penetration condition

$$\sum_{j=1}^{N} A_{ij} \, G_j = (\vec{V}_{ls} - \vec{V}_w)_i \cdot \vec{n}_i \quad \text{for } i = 1,2,\ldots,N \qquad (4.7)$$

where N is the total number of the elements representing the wing, and the A_{ij} represent the normal component of the velocity at the control point of the ith (receiving) element generated by a closed loop of unit circulation around the jth (sending) element. At the ith control point $(V_{ls} - V_w)_i$ is the velocity of the lifting surface minus the velocity induced by the wake elements.

For a rigid wing, the problem is posed in a moving coordinate system attached to a reference configuration of the wing and the A_{ij} are constant. For an elastic wing the A_{ij} must be computed at each time step.

4.2.6 The unsteady Kutta condition

The Kutta condition requires ΔC_p to be zero along the wing tips and trailing edge. It is satisfied at each time step by convecting the vorticity along the sharp edges of the wing into the wake at the local particle velocity. Each node is displaced according to

$$\Delta \vec{r} = \vec{v} \, \Delta t \qquad (4.8)$$

where $\Delta \vec{r}$ is the displacement of the node, $\vec{v}$ is the local velocity relative to the moving coordinate system, and Δt is the time step. The local particle velocity is computed from

$$\vec{v} = \vec{V} - \vec{V}_A - \vec{\omega} \times \vec{r} \qquad (4.9)$$

where $\vec{V}$ is the absolute velocity calculated from the Biot-Savart Law. To maintain the wake in a force-free position, each node in the wake is also displaced according to Equations (4.8) and (4.9).

4.3 The Impulsive Start of the UVLM

Initially, the wing is represented by a lattice. There is no wake. Before motion begins all circulations are zero. The instant motion begins the circulations in the bound vortex lattice change. A discrete vortex line forms along the wing tips and trailing edge. The

existence of this starting vortex is dictated by the requirement of spatial conservation of circulation. This is the vorticity that is convected into the wake from the sharp edges of the wing at the particle velocity.

The entire aeroelastic model has been nondimensionalized by defining a characteristic length, ℓ_c, and characteristic velocity, U_∞. From these definitions the nondimensional time step, $\Delta\tau$, is defined as ℓ_c/U_∞. As much as possible, it is desirable to have uniform elements in the lattices. To achieve this end, we choose the characteristic length to be the chord of the rectangular elements. At each time step the free-vortex system is convected at the local particle velocity, Equation (4.8). As a result the streamwise lengths of the wake elements are approximately the same as the bound elements. One might also note that an increase in the number of chordwise elements is accompanied by a corresponding decrease in the actual time step.

4.4 Graphical Representations of the Flowfield

In Figure 4.2 a flowfield predicted by the general UVLM is illustrated. The wing-tip vortex system is clearly evident. It strongly influences the velocity at the control points along the wing tips. In Figure 4.3 the flowfield is shown in different views. In Figure 4.4 the strength of the vorticity fields of both the bound and free vortex sheets is shown.

4.5 The Aerodynamic Loading

The aerodynamic loading is determined by calculating the pressure jump across each individual element in the bound (wing) lattice. The
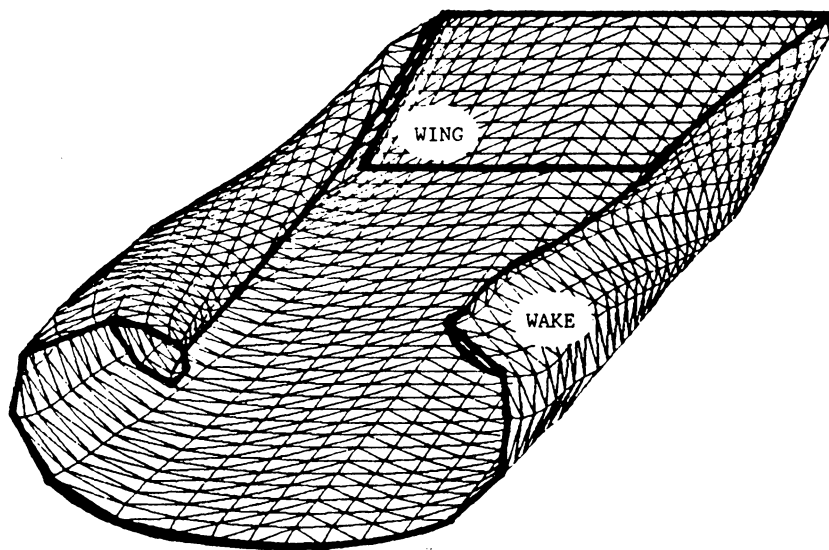
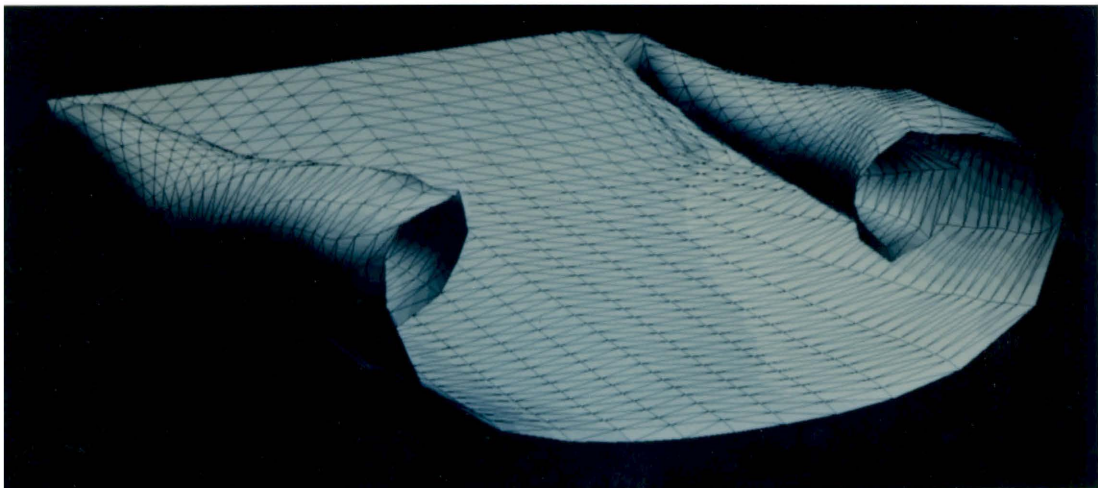Figure 4.2. Wireframe of Wing and Wake Lattice.
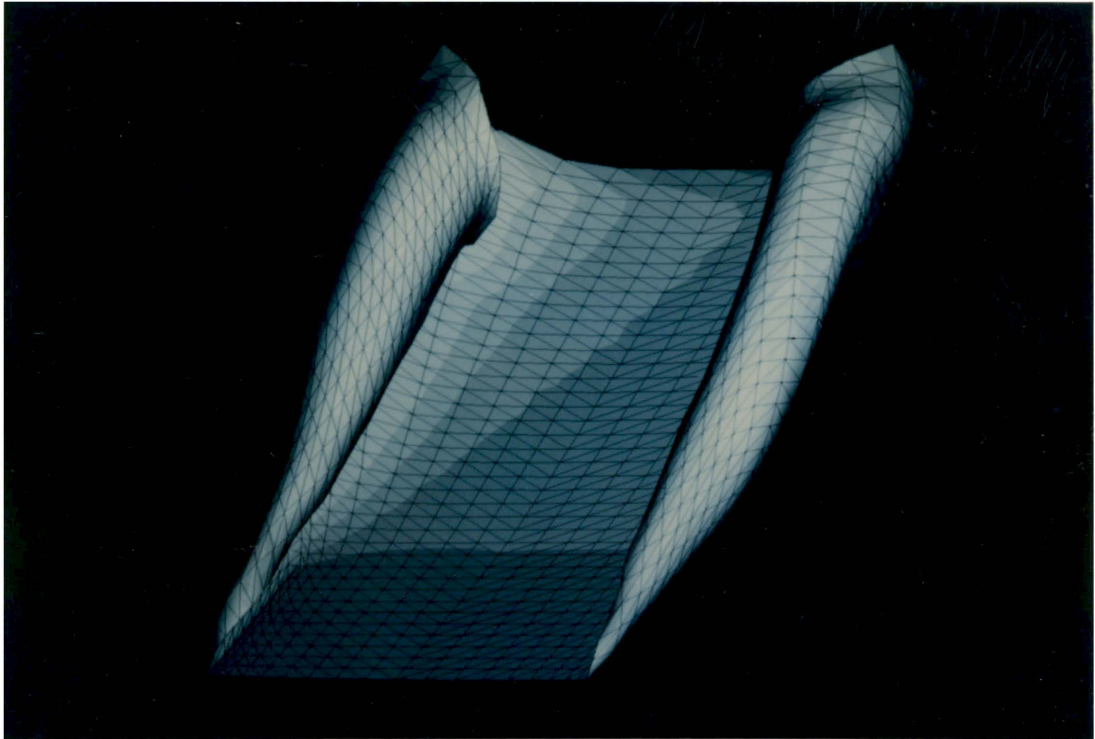
Figure 4.3. Vortex-Lattice Representations.
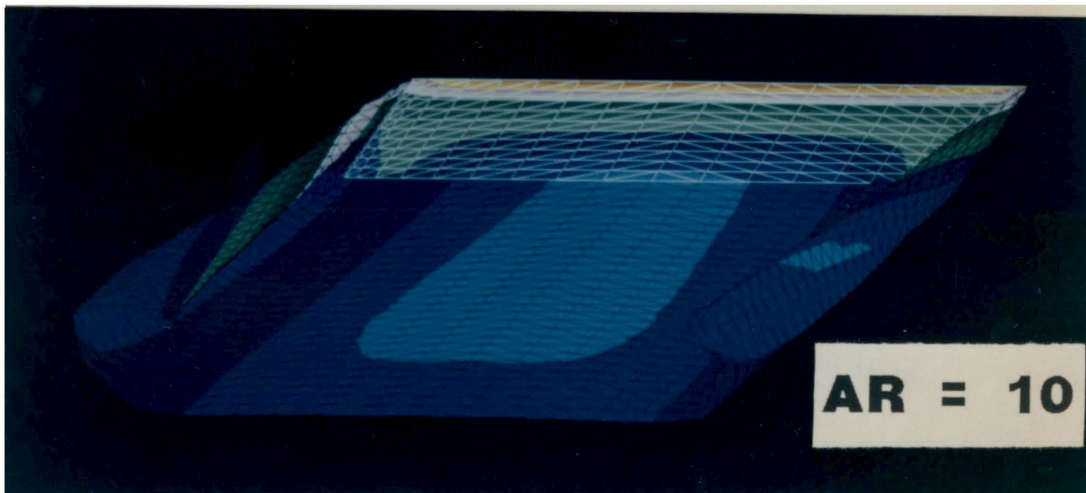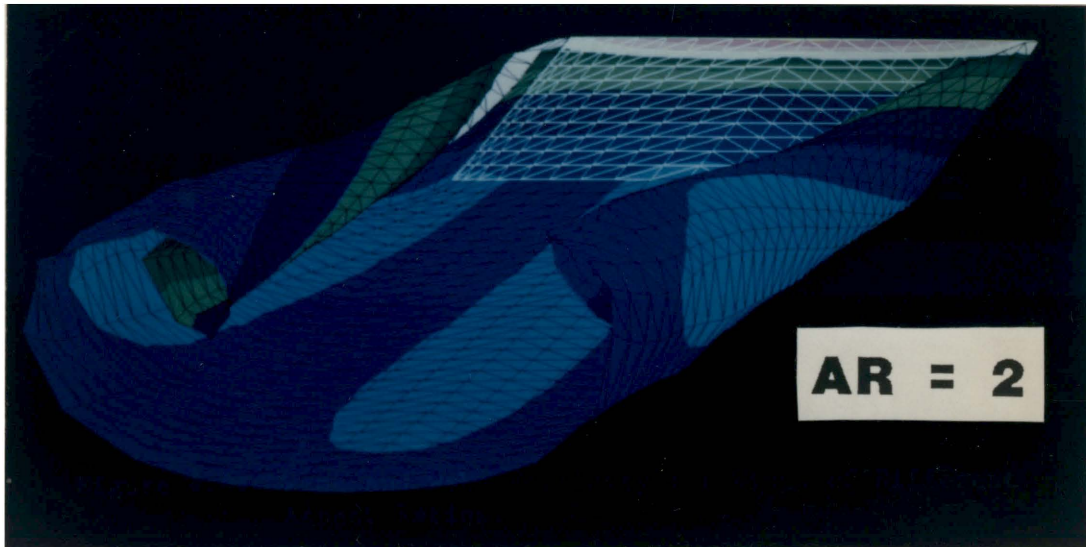
Figure 4.4. Wing and Wake Vorticity for Wings of Different
Aspect Ratios.

pressure is calculated from Bernoulli's equation for unsteady flows. The pressure difference between the upper and lower surface of element i is given by

$$\Delta C_{p_i} = -2 \frac{\partial G_i}{\partial t} - 2[\Delta\vec{V} \cdot (\vec{V} - \dot{\vec{R}} - \vec{\omega} \times \vec{r})] \qquad (4.10)$$

where $\Delta\vec{V}$ is the discontinuity in the tangential component caused by the local vorticity. The average circulation around the discrete vortex segments on parallel edges of an element is considered to be the circulation around a sheet of vorticity parallel to and between the same edges. The vorticity is concentrated into cores to facilitate computation of the velocity field. The average circulation is related to the jump in the tangential component of velocity perpendicular to these edges, across the thickness of the lifting surface. The reader is again referred to Konstadinopoulos (1981).

The pressure distribution is multiplied by the area of the element to provide the elemental force perpendicular to the surface. These forces are integrated along the chord and span to provide the aerodynamic forces and moments.

CHAPTER V

THE NUMERICAL SOLUTION SCHEME

5.1 Overview

The equations governing the motion of the structure have been de-
veloped. In addition, the model that determines the motion-dependent
aerodynamic loads has been described. The interaction between these
aerodynamic loads and wing motion presents an interesting challenge
since the loads are necessary to predict the motion, yet the motion is
necessary to predict the loads. Therefore, an interacting numerical
integration scheme has been developed, which determines the motion,
loads, and wing/wake geometry simultaneously. The method is based on
Hamming's Predictor-Corrector Method as described in Carnahan (1969).

This integration technique coupled with the nondimensionalized
form of all governing equations results in a reliable arrangement of
the problem. The characteristic length, ℓ_c, is the chordwise length
of a lattice element. One time step is represented by the time neces-
sary for a fluid particle to convect approximately one ℓ_c. The
predictor-corrector method does not subdivide a time step of integra-
tion as do other techniques such as Runge-Kutta. Hence, the chordwise
size of the convected elements remains nearly uniform for all
calculations of the loads.

5.2 The First-Order Differential Equations

The development of the two-degree-of-freedom model for the rigid
wing and the multiple degree-of-freedom model for the elastic wing

49

both result in a set of first-order differential equations as developed in previous sections. The set of first-order equations which describe the two-degree-of-freedom motion (see Eqs. (2.15) and (2.16)) can be written as

$$\dot{\eta} = \frac{1}{K - r^2 \cos^2(\alpha + \phi)} \left[(K_\alpha \alpha + C_\alpha \xi - nCC_m)r \cos(\alpha + \phi) \right.$$

$$\left. + K\{\xi^2 r \sin(\alpha + \phi) - K_y Y - C_y \eta - CC_n \cos(\alpha + \phi)\} \right] \qquad (5.1)$$

$$\dot{\xi} = \frac{1}{K - r^2 \cos^2(\alpha + \phi)} \{(C_y \eta + K_y Y)r \cos(\alpha + \phi)$$

$$- r^2 \xi^2 \sin(\alpha + \phi) \cos(\alpha + \phi) - (C_\alpha \xi + K_\alpha \alpha)$$

$$+ C(n C_m + r \cos^2(\alpha + \phi)C_n)\} \qquad (5.2)$$

where

$$\dot{Y} = \eta \qquad (5.3)$$

$$\dot{\alpha} = \xi \qquad (5.4)$$

The equations of motion for the elastic wing are repeated for convenience.

$$\begin{Bmatrix} \{\dot{\eta}\} \\ \{\dot{q}\}_d \end{Bmatrix} = \begin{bmatrix} 0 & -[M]^{-1}[K] \\ [I] & 0 \end{bmatrix} \begin{Bmatrix} \{\eta\} \\ \{q\}_d \end{Bmatrix} + \begin{Bmatrix} [M]^{-1} \{A\}_d \\ 0 \end{Bmatrix} \qquad (3.34)$$

In general, we have a system of first-order differential equations of the form

$$\frac{dY_1}{dt} = f_1(t, Y_1, Y_2, \ldots, Y_n)$$

$$\frac{dY_2}{dt} = f_2(t, Y_1, Y_2, \ldots, Y_n)$$

$$\vdots$$

$$\frac{dY_n}{dt} = f_n(t, Y_1, Y_2, \ldots, Y_n)$$

(5.5)

where n is 4 for the two-degree-of-freedom problem and n is twice the number of modes for the elastic wing problem.

5.3   The Basic Predictor-Corrector Method

In both sets of equations the right-hand side represents the derivatives of the dependent variables. The general predictor-corrector scheme requires the values of the dependent variables at the current and three previous time steps. In addition, the derivatives at the current and two previous time steps are required. With this information the computation of the state variables for the next time step can be calculated. The approach to obtaining the information necessary to start the procedure will be described later in this chapter. The integration of one time step will be described when all the necessary information is known.

The state variables at the end of the current time step are pre-
dicted by the following equation:

$$y_{j,i+1,0} = y_{j,i-3} + \frac{4}{3} \Delta t(2f_{j,i} - f_{j,i-1} + 2f_{j,i-2}) \qquad (5.6)$$

$$j = 1,2,\ldots,n$$

where the subscript i is the index for the time step and the sub-
script 0 signifies the initial prediction of the state variables.
The time interval, Δt, is unity in our formulation due to the non-
dimensionalization. The local truncation error, $e_{j,i}$, is estimated
at the end of each time step and this truncation error is used to
modify the predicted values to y^*.

$$y^*_{j,i+1,0} = y_{j,i+1,0} + \frac{112}{9} e_{j,i} \qquad (5.7)$$

Then y^* is used to obtain the derivatives (f^*). Next, the
"corrector" equation is used to obtain the updated state variables.

$$y_{j,i+1,M} = \frac{1}{8} [9y_{j,i} - y_{j,i-2}$$

$$+ 3\Delta t(f^*_{j,i+1,M-1} + 2f_{j,i} - f_{j,i-1})] \qquad (5.8)$$

The corrector equation is used iteratively (M is the index for
this iteration) until convergence on the state variables is achieved.
The derivatives, $f^*_{j,i+1,M-1}$, are computed from $y_{j,i+1,M-1}$. Hence,
the corrector equation uses the current information. In addition, it
is important to note that the aerodynamic model is used each time the
state variables are predicted or corrected.

The wake is convected from the position generated at the end of the last time step into the new position. This wake, new state variables, and wing geometry are used to compute the loads. Therefore, the aerodynamic loads are current.

Once convergence of the state variables and loads has been achieved the local truncation error is estimated.

$$e_{j,i+1} = \frac{9}{121} (y_{j,i+1,M} - y_{j,i+1,M-1}) \qquad (5.9)$$

A final modification is made to the state variables.

$$y_{j,i+1} = y_{j,i+1,M} - e_{j,i+1} \qquad (5.10)$$

5.4 Starting the Predictor-Corrector Method

The predictor-corrector procedure requires the derivatives of the dependent variables from the current and three previous time steps. It also requires the derivatives of these variables for the current and two previous steps. Carnahan suggests a Runge-Kutta scheme to determine these values as a starter for the predictor-corrector technique. We elect to use a Taylor series expansion to establish the starting values because this approach only requires the aerodynamic loads at integral time steps.

For the nth equation

$$\frac{dY_n}{dt} = f_n(t, Y_1, Y_2, \ldots, Y_n) \qquad (5.11)$$

where the right-hand side of Equation (5.11) is the right-hand side of Equations (5.1) through (5.4), or (3.34). Then, Equation (5.11) is expressed in difference forms between the 1st and 2nd time step.

$$\frac{Y_{n_2} - Y_{n_1}}{\Delta t} = f_{n_1}(t, Y_1, Y_2, \ldots, Y_n) \tag{5.12}$$

or

$$Y_{n_2} = f_{n_1}(t, Y_1, Y_2, \ldots, Y_n) * \Delta t + Y_{n_1} \tag{5.13}$$

Now recall,

$$Y(t + \Delta t) = Y(t) + \Delta t\, Y'(t) + \frac{\Delta t^2}{2!} Y''(t) + h.o.t. \tag{5.14}$$

where the prime indicates differentiation and h.o.t. represents the higher-order terms. Therefore,

$$Y_{n_3} = Y_{n_2} + \Delta t\, Y'_{n_2} + \frac{\Delta t^2}{2} Y''_{n_2} + h.o.t. \tag{5.15}$$

or, considering Equation (5.11), Equation (5.15) becomes

$$Y_{n_3} = Y_{n_2} + \Delta t\, f_{n_2} + \frac{f'_{n_2}\, \Delta t^2}{2!} + h.o.t. \tag{5.16}$$

Approximating from Y_{n_1} for $2\Delta t$ and considering relation (5.14)

$$Y_{n_3}(t + 2\Delta t) = Y_{n_1} + 2\Delta t\, Y'_{n_1} + \frac{(2\Delta t)^2 Y_{n_1}}{2!} + h.o.t. \tag{5.17}$$

or

$$Y_{n_3} = Y_{n_1} + 2\Delta t \, f_{n_1} + 2\Delta t^2 f'_{n_1} + h.o.t. \qquad (5.18)$$

If we multiply Equation (5.16) by 4 and subtract Equation (5.18) we obtain

$$3Y_{n_3} = 4Y_{n_2} - Y_{n_1} + 4f_{n_2} \Delta t - 2f_{n_1} \Delta t + h.o.t. \qquad (5.19)$$

Next we make the approximation $f'_{n_2} \simeq f'_{n_1}$; then Equation (5.19) can be rewritten as

$$Y_{n_3} = \frac{4}{3} Y_{n_2} - \frac{Y_{n_1}}{3} + \left(\frac{4}{3} f_{n_2} - \frac{2}{3} f_{n_1} \right) \Delta t + h.o.t \qquad (5.20)$$

In a similar fashion an expression for Y_{n_4} is developed

$$Y_{n_4} = \frac{4}{3} Y_{n_3} - \frac{Y_{n_2}}{3} + \left(\frac{4}{3} f_{n_3} - \frac{2}{3} f_{n_2} \right) \Delta t + h.o.t. \qquad (5.21)$$

Hence, the starting values for the general predictor-corrector procedure are available.

The integration of the equations of motion by the predictor-corrector method is the same for both the rigid wing on the elastic foundation and the elastic wing on the rigid support. However, the complete integration process includes the interaction with the aerodynamic model; hence, differences may exist in the complete integration process. The convection of vorticity from the wing is performed in the wing-fixed (not inertial) reference frame. Therefore, the

basic difference in the integration process is whether or not the reference system is moving and the associated effect on the convection of the flowfield at the local velocity. Interestingly, the two-degree-of-freedom rigid wing presents a more complicated integration process than the multiple-degree-of-freedom elastic wing since the elastic wing is assumed to be cantilevered from a fixed support and the rigid wing is attached to a rotating support. The complete integration procedures will be described.

5.5 Integration Method for the Rigid-Wing System

5.5.1 First-order convection theory

The integration technique for the equations developed for the rigid wing is illustrated by the flowchart in Figure 5.1. First, new state variables are predicted. These variables represent both static and dynamic contributions. Next, the wake is convected to the new force-free position from the position generated at the end of the last time step and the aerodynamic loads are computed. Then, the state variables are corrected. It is important to note that the aerodynamic model is used each time the state variables are predicted or corrected. Convergence of both the state variables and the aerodynamic loads is required. If convergence is not achieved the flowfield is convected from that generated (and converged) at the previous time step, new aerodynamic loads are determined, and the state variables are again corrected. Convergence is checked. If convergence is achieved then the conditions for the beginning of the next time step are known.
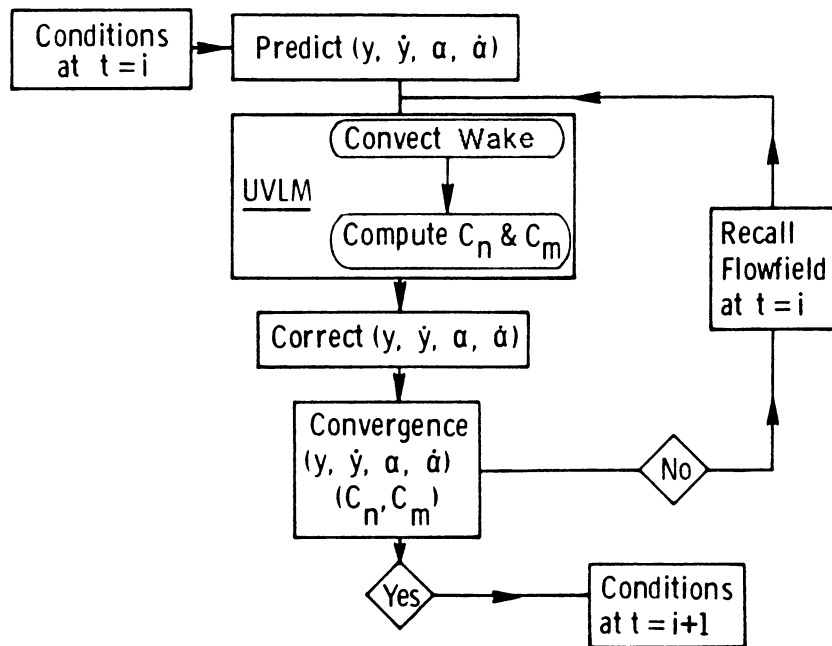
Figure 5.1. Flowchart of the Integration Scheme Using Lower-
Order Convection Theory, Rigid-Wing Formulation.

5.5.2 Second-order convection theory

A higher-order convection strategy was examined (see Fig. 5.2).
In this approach, a two stage corrector process was developed. In
stage one, the motion was corrected and the aerodynamic loads deter-
mined for a wake in a fixed position. That is, the position of the
wake was not recomputed each time the state variables were determined.
Stage one was repeated to convergence of both the loads and motion.
In stage two, the wake was convected by an iterative process to a con-
verged position with fixed state variables. Then, the field points
for the wake were convected at a velocity based upon the average of
the corrected variables and the variables from the previous time step.
The new position of the wake is checked for convergence with the pre-
vious position. A new two-stage cycle begins: this new wake was used
for stage one (motion and loads determined) and the converged new
motion and loads were then used again for stage two (wake position).
Motion, loads, and the wake were required to converge before the
integration process continued to the next integration time step. The
computational time was increased five-fold; however, the predicted
results showed no discernible differences over the lower-order con-
vergence scheme.

5.6 Solution of the Equations for the Elastic Wing

5.6.1 Static solution

The solution of the equations for the elastic wing is handled in
a somewhat different manner. The static solution of the elastic wing
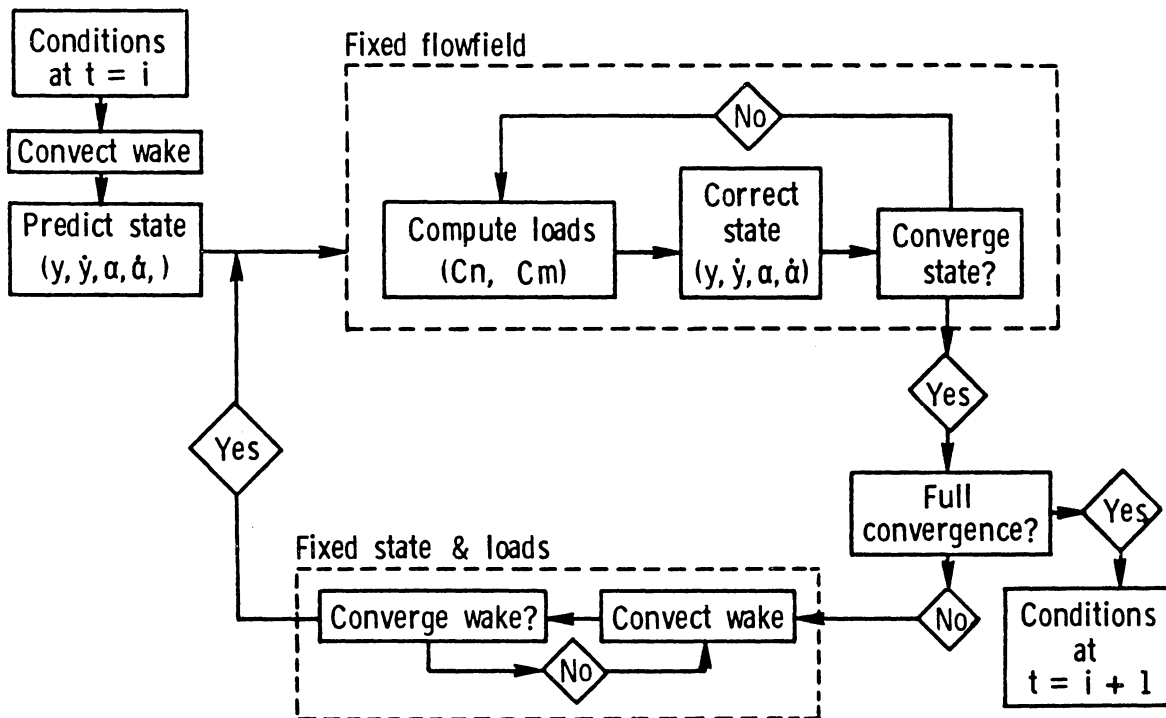is required prior to the start of the dynamic solution. The analysis

Figure 5.2. Flowchart of the Integration Scheme Using Second-Order Convection Theory, Rigid-Wing Formulation.

of the static problem begins with the specification of a nominal angle

of attack. The corresponding distributed steady aerodynamic loads are

computed. This load and the weight are then used to calculate the

bending and torsional deflections. At this point the wing has a new

shape, but the loads still correspond to the old shape. New loads,

corresponding to the new shape, are obtained next; then the corre-

sponding new shape is obtained. The procedure is repeated until

either both the shape and loads converge or aeroelastic divergence

(where the aerodynamic forces exceed the elastic restoring forces)

occurs. The procedure is illustrated in Figure 5.3. The elements

with dots at their centroids are part of the bound lattice (wing); the

others are part of the free lattice (wake).

5.6.2 Dynamic solution

The integration technique which provides the dynamic solution is

illustrated in Figure 5.4. Similarities do exist with the rigid wing

formulation. The wake is convected to the new force-free position

from the position generated at the end of the last time step. Unlike

the rigid-wing formulation, this convection is only performed once.

The new state variables are predicted for the first integration pass

and are corrected for all subsequent passes. These state variables

only represent the dynamic contribution. They are added to the static

contribution and are used through the modal expansions to generate the

new wing shape. The wake, new state variables, and wing geometry are

used to compute the loads. Therefore, the aerodynamic loads are

current. It is important to note that the aerodynamic model is used
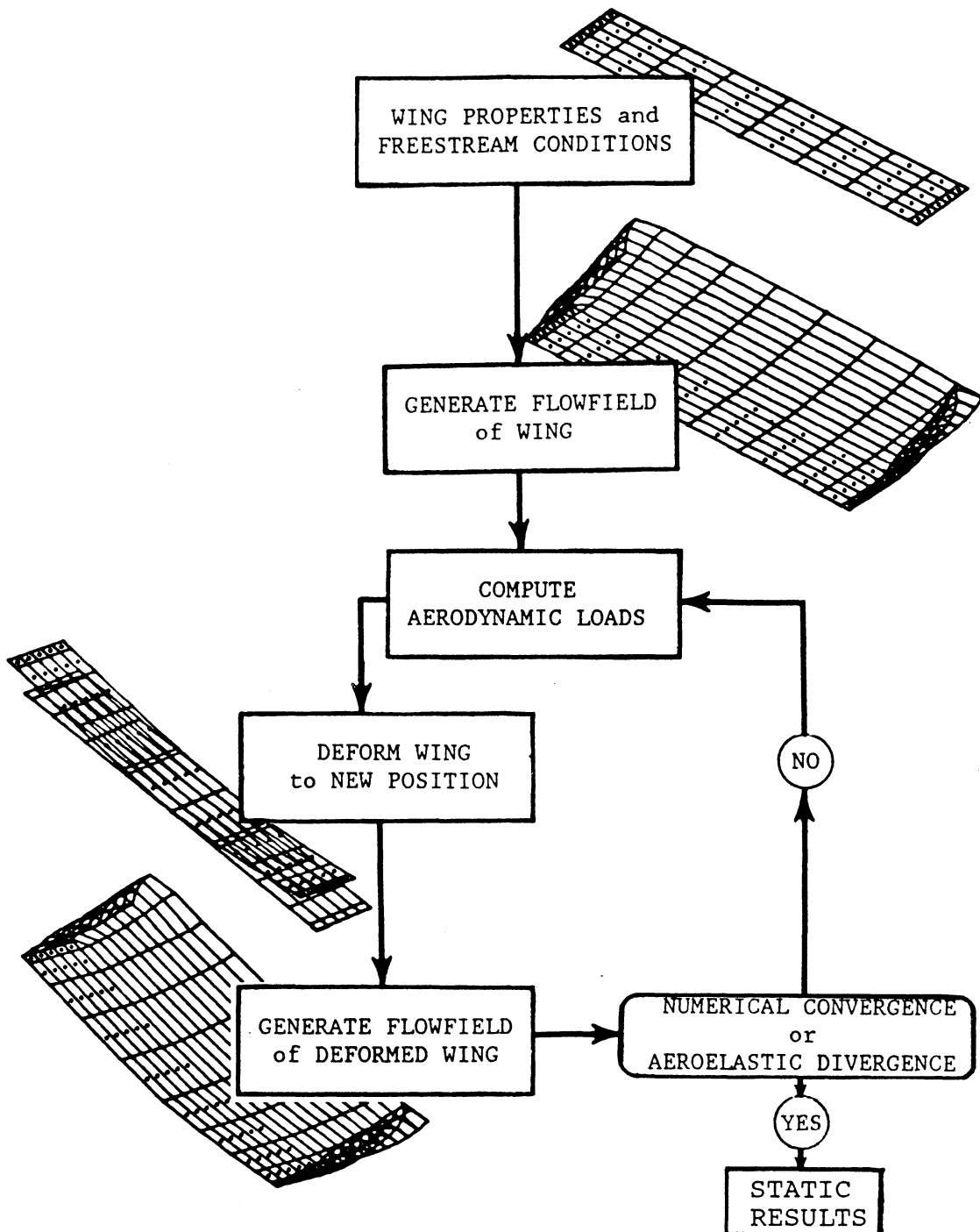
Figure 5.3. Flowchart for the Determination of the Elastic
Wing Deformations Due to Static Loads.
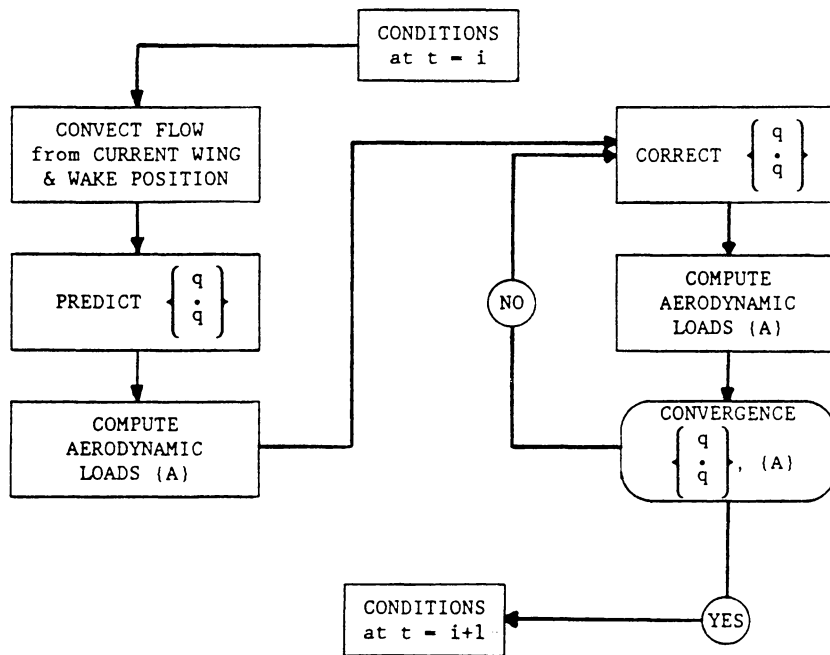
Figure 5.4. The Integration Process for the Equations Governing the Dynamic Solution of the Elastic Wing.

each time the state variables are predicted or corrected. The state variables are corrected, new wing geometry is computed, the aerodynamic loads are updated, and convergence of both the state variables and aerodynamic loads are checked. If convergence is not achieved the scheme returns to the corrector stage. Convergence is required of motion and loads at the end of each time step prior to advancing.

CHAPTER VI

APPLICATION OF THE MODEL TO SPECIFIC EXAMPLES

6.1 Introduction

In this chapter, the aeroelastic model is used with several exam-
ples to demonstrate the technique. These examples include cases for

the rigid wing on an elastic support and the elastic wing on a fixed

support. These examples illustrate the ability of the technique to

predict the aeroelastic behavior and the unsteady aerodynamic loads of

a wing.

6.2 An Example of Aeroelastic Behavior for the Rigid Wing

First, we consider an example that is similar to one discussed

by Fung. A large-aspect-ratio wing that can only plunge and pitch

about the elastic axis is placed in a uniform steady flow. A cross-

sectional view of this wing is shown in Figure 2.1.

Fung's model for the aerodynamic loads is limited to two-

dimensional flow. Our model includes the effect of the wing tips and

the wake; hence, these predicted results account for three-dimensional

and unsteady characteristics. The essential physical properties for

this example are given in Table 6.1 (these are values used by Fung).

No structural damping is present in this example; therefore,

damping of the motion results strictly from aerodynamic effects.

Later, we will demonstrate the additional effect that structural

damping contributes to the wing response. In addition, the elastic

axis and the mass axis are coincident; hence, the pitch and plunge

degrees of freedom are not coupled inertially. The coupling which

Table 6.1. Properties of the Rigid Wing Example

Wing area	60 ft^2
Wing chord	60 ft
Elastic axis/mass axis offset	0
Elastic axis location (% of chord)	50%
Mass of wing	269 $\frac{\text{lb sec}^2}{\text{ft}}$
Mass moment of inertia	150630 lb sec^2 ft
Support translational spring stiffness	208.5 lb/ft
Support torsional spring stiffness	363020 ft lb/rad
Translational natural frequency	.880 rad/sec
Torsional natural frequency	1.552 rad/sec
Density of air	.002378 lb sec^2/ft^4

occurs between the degrees of freedom is a result of aerodynamic effects.

Two different freestream speeds are considered for the example and the density of air at sea level is used. These conditions are chosen to bound the critical dynamic pressure which we define as the dynamic pressure at which the motion neither grows nor decays. This critical dynamic pressure results in wing flutter.

Typically, for the two-degree-of-freedom model, a simulation is performed by establishing the flowfield for a wing which is fixed at a static angle of attack. Next, the wing is released from this fixed position and given an initial disturbance. The response of the wing is examined; a decay of motion in both degrees of freedom indicates stability and a growth in motion indicates instability.

6.2.1 Subcritical response without structural damping

In Figure 6.1 we show the response of the wing to a small initial disturbance which has the following form:

$$Y(0) = 0 \qquad \dot{Y}(0) = 0.01$$

and $\qquad\qquad\qquad\qquad\qquad\qquad\qquad\qquad\qquad\qquad\qquad$ (6.1)

$$\alpha(0) = 0 \qquad \dot{\alpha}(0) = 0.02$$

The freestream speed for this case is small and results in a dynamic pressure which is less than the critical dynamic pressure. The displacements and velocities associated with both degrees of freedom clearly decay with time. The pitch and plunge displacements reflect
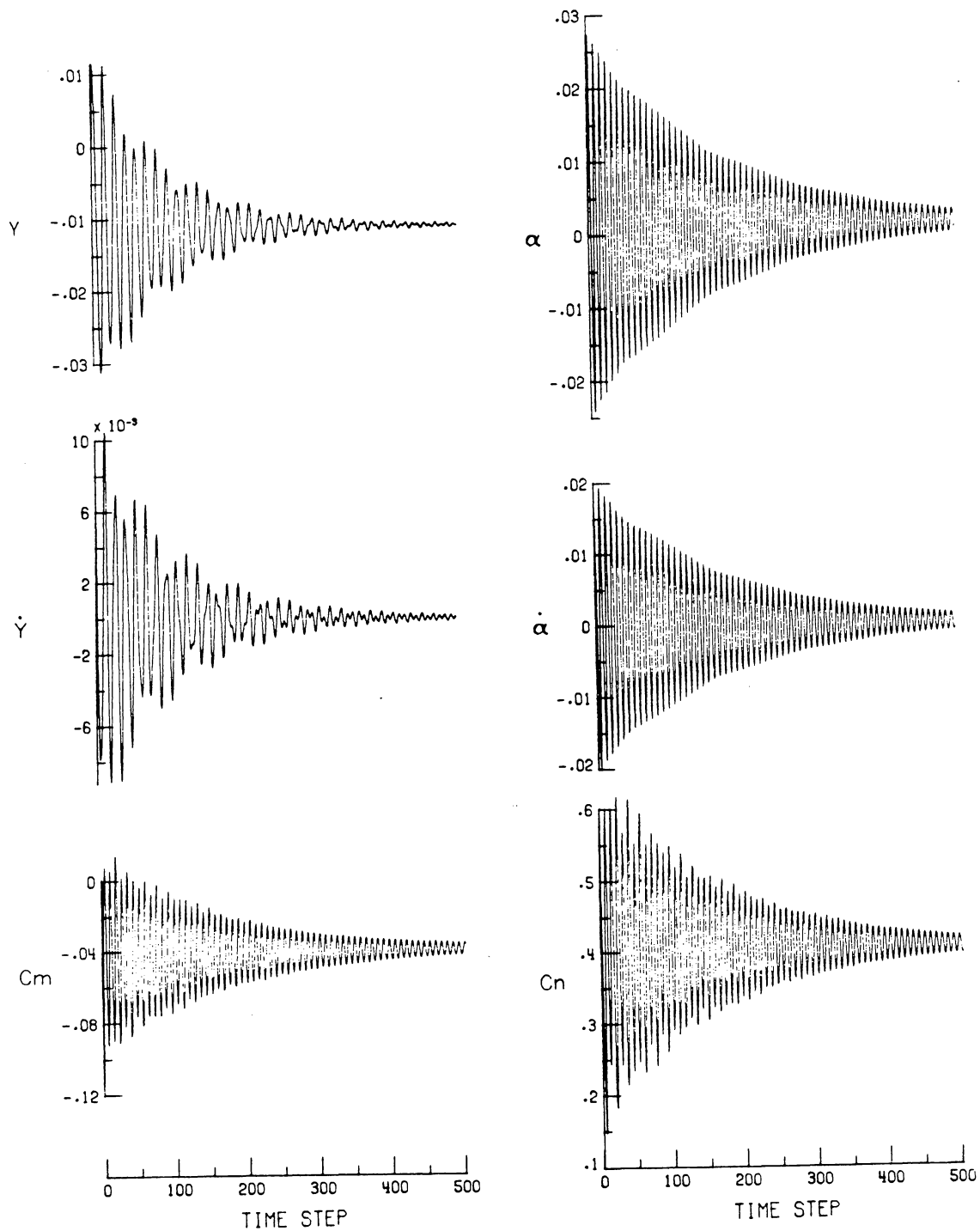
Figure 6.1. Response of the Rigid Wing at a Subcritical
Dynamic Pressure.

the static and dynamic contribution; hence, in time the motion will decay and will eventually converge to the static (which includes the effects of both aerodynamic and mass induced loading) condition.

In addition, as one would expect, the frequency of oscillation for each degree of freedom closely matches the uncoupled frequencies of oscillation associated with the respective elastic springs. The aerodynamic normal-force and pitching-moment coefficients are also shown. This aerodynamic loading decays to the steady aerodynamic loads.

As a matter of interest, in nondimensional form the frequencies are dependent upon the freestream speed; therefore, a change in the freestream speed will change the nondimensional frequency of oscillation. However, for subcritical conditions the frequency in physical time would remain nearly constant. Also, referring to the nondimensional form of the governing equations of motion (see Chapter II, Eqs. (2.15) and (2.16)) one finds that the stiffness of the support spring is reduced as the freestream speed is increased – in fact, the square of the speed appears in the denominator. The nondimensional structural damping, if present, is inversely proportional to the freestream speed.

6.2.2 Supercritical response to a small initial disturbance

Next, we show the response of the wing to a dynamic pressure that is larger than the critical dynamic pressure. The initial conditions are the same (see Eqs. (6.1)) as those used in the previous case. The

time histories of both degrees of freedom and their time derivatives
are shown in Figure 6.2.

The initial disturbance grows and, as we will show, can be ex-
pected to reach a limit cycle eventually. A gradual transition occurs
very early in the motion and is noticed in the response associated
with the plunge degree of freedom. The motion for the two degrees of
freedom changes from the natural frequencies in these modes to a com-
mon frequency, which is nearly the frequency of flutter in the limit
cycle. This common frequency lies between the two natural frequencies
and is closer to the natural frequency in pitch than to the one in
plunge – a characteristic of the flutter phenomenon which has been
well documented. The time histories of the aerodynamic normal load
and pitching moment coefficients are also shown. It must be empha-
sized that the aerodynamic loads and wing motion are dependent upon
each other and a form of the solution for the loads or motion is not
assumed. At each time step, the integration process iterates to a
converged solution, predicting both the flowfield and the motion of
the wing simultaneously.

6.2.3 Supercritical response to a large initial disturbance

In Figure 6.3, we show the response of the wing to a large
initial disturbance which has the following form:

$$Y(0) = 0 \qquad \dot{Y}(0) = 1.0$$

and $\qquad\qquad\qquad\qquad\qquad\qquad\qquad\qquad\qquad\qquad$ (6.2)
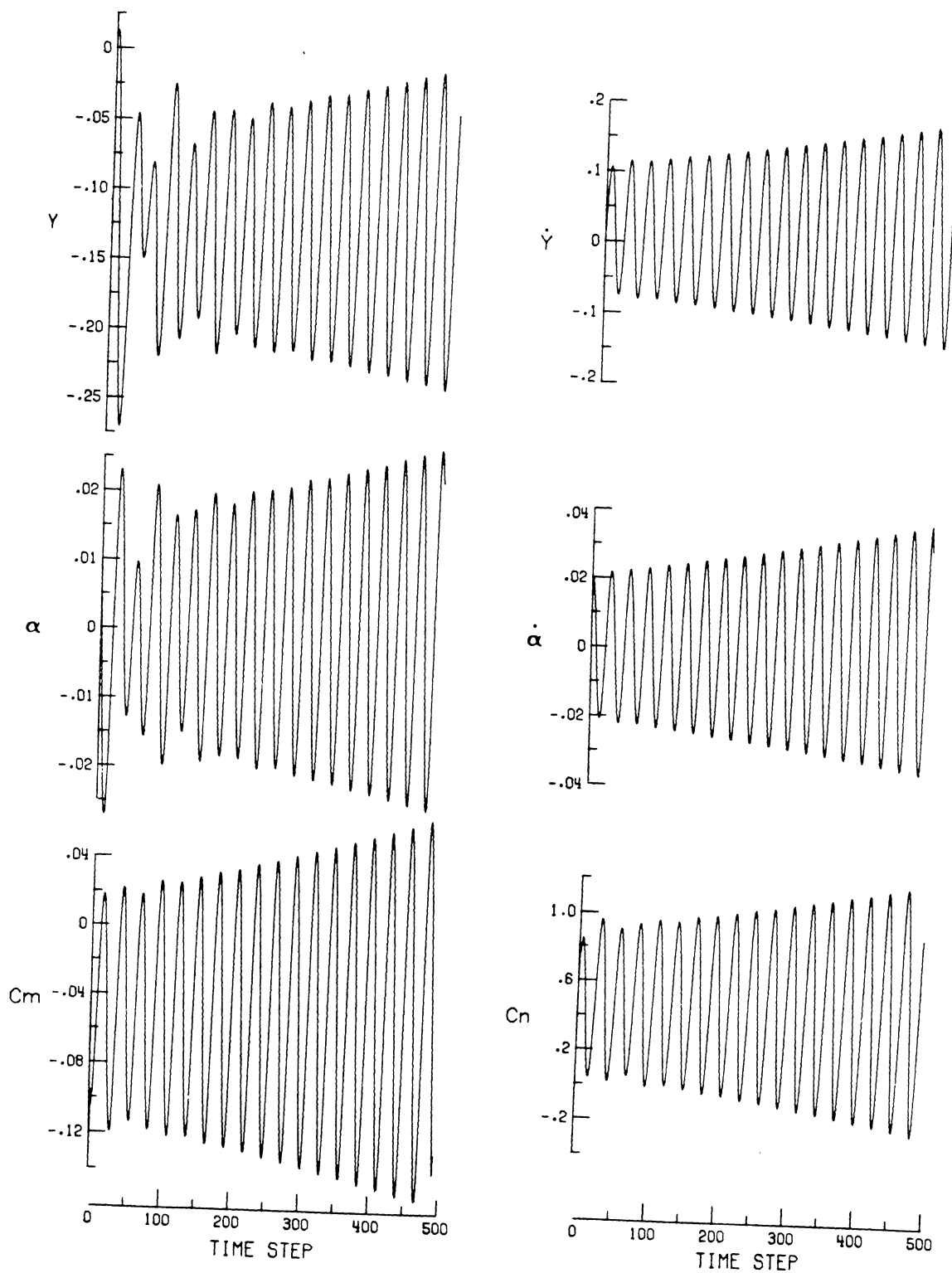
$$\alpha(0) = 0 \qquad \dot{\alpha}(0) = 0$$

Figure 6.2. Response of the Rigid Wing at a Critical Dynamic
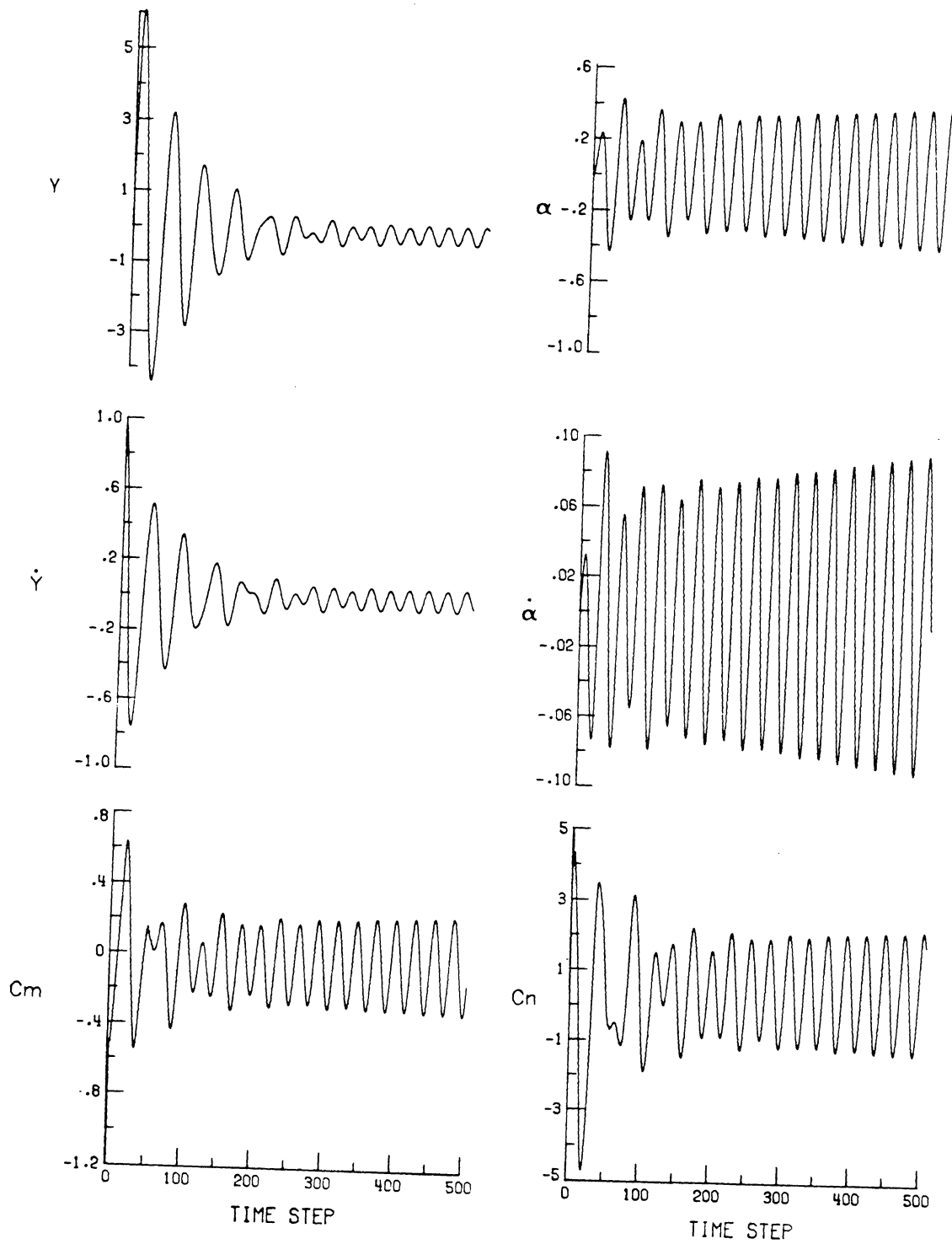Pressure – Small Initial Conditions.

Figure 6.3. Response of the Rigid Wing at a Critical Dynamic Pressure - Large Initial Conditions.

The dynamic pressure is the same as the previous case. However, in this case we introduce a larger initial disturbance to only the plunge degree of freedom.

The equations of motion are uncoupled in the absence of aerodynamic loads since $r = 0$. Yet, we find that the pitch is strongly excited almost immediately, which is clearly the result of coupling introduced by the aerodynamic loads. The plunging motion rapidly decays. In this case, the transition of the motion to a common frequency is clearly evident. The delay in this transition (when compared to the case with the small initial disturbance) is created by the large initial condition.

After the initial rapid decay, the plunging motion appears to approach a limit cycle, not to decay to zero. The pitching motion continues to grow in time. Presumably, independent of the different initial disturbances introduced in these cases, the pitching and plunging motion of these two cases will eventually match. In Figure 6.4, we show the phase planes for the two cases shown in Figures 6.2 and 6.3. If we examine the phase planes associated with the plunge motion, we observe that in the upper half of Figure 6.4 the small motion appears to be growing around an unstable focus towards a limit cycle, while in the lower half of the figure the large motion appears to be decaying toward the same limit cycle.

6.2.4 Subcritical response with structural damping

No structural damping in the support is included in these previous results, though aerodynamic damping is modelled by the UVLM.
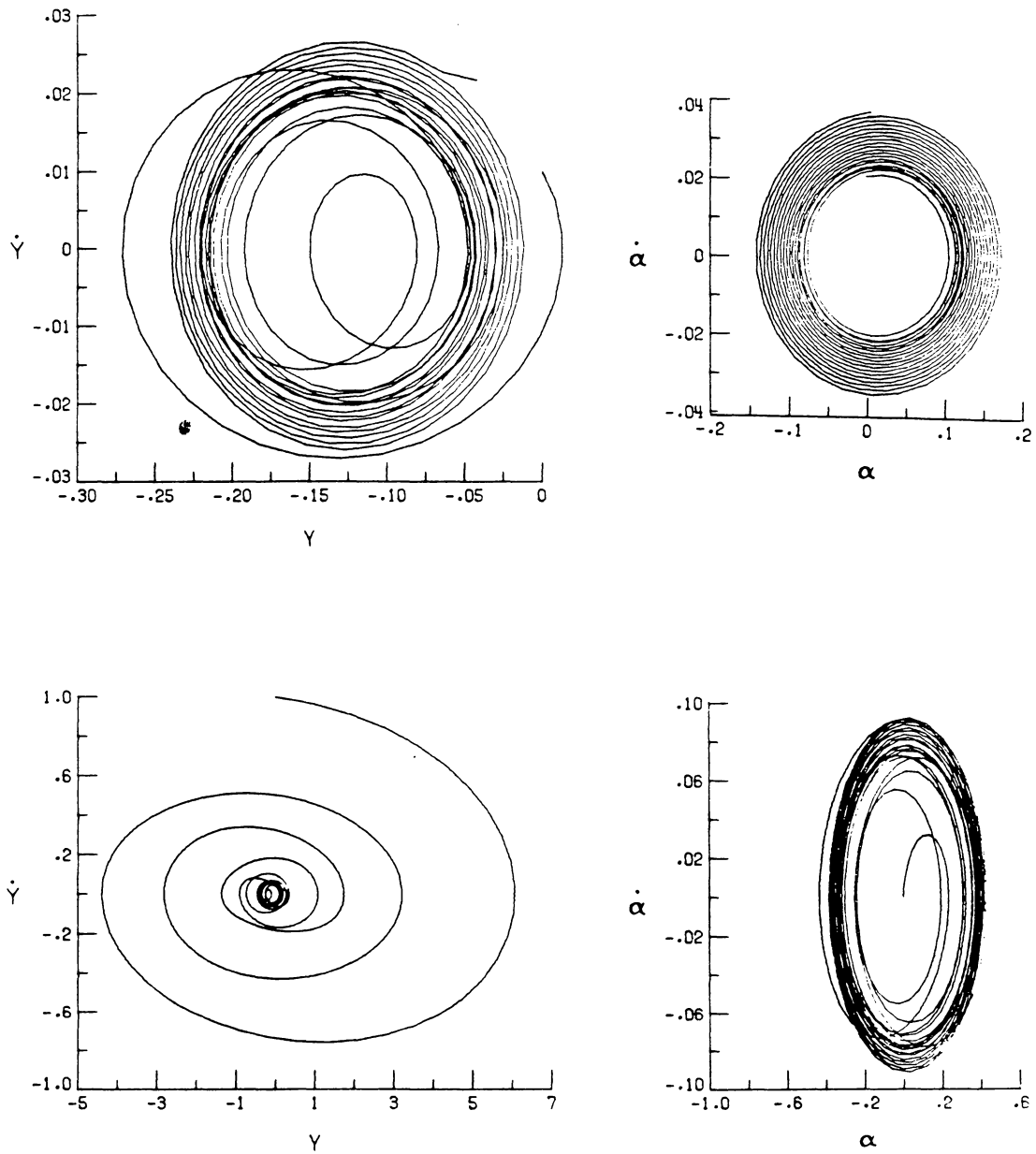
Figure 6.4. Phase Plane Diagrams at the Critical Dynamic
Pressures - Small and Large Initial Conditions.

In fact, in some frequency domain solutions, the damping coefficient is used as an index to determine the onset of flutter. The present method can also account for damping in the support. In addition, the present equations of motion can be readily extended to include non-linear stiffness and damping for both degrees of freedom thereby providing a means to study nonlinear structural behavior.

In Figure 6.5, we show the response to the same initial conditions and same dynamic pressure as used in the case reflected in Figure 6.2. However, we now introduce structural damping into the problem, for the case illustrated $C_y = C_\alpha = 0.01$. Now instead of growing, the initial disturbances decay and the wing does not flutter. As one might expect, the flutter boundary is quite sensitive to structural damping.

6.2.5 Comparison with theoretical results

The unstable results discussed above were obtained by using a wind speed of 125 feet per second, and the stable results were obtained using a wind speed of 40 feet per second. The density of air at sea level was used and assumed constant. The critical speed lies between these two. Suggested methods for extracting the exact critical velocity will be discussed later. Fung found the critical velocity to be 162 feet per second which is higher than our predicted value. The differences in the two approaches are (1) Fung considered an infinite aspect ratio, and we consider an aspect ratio of ten which introduces finite wing effects; (2) Fung considered a zero static angle of attack, and we consider three degrees which introduce
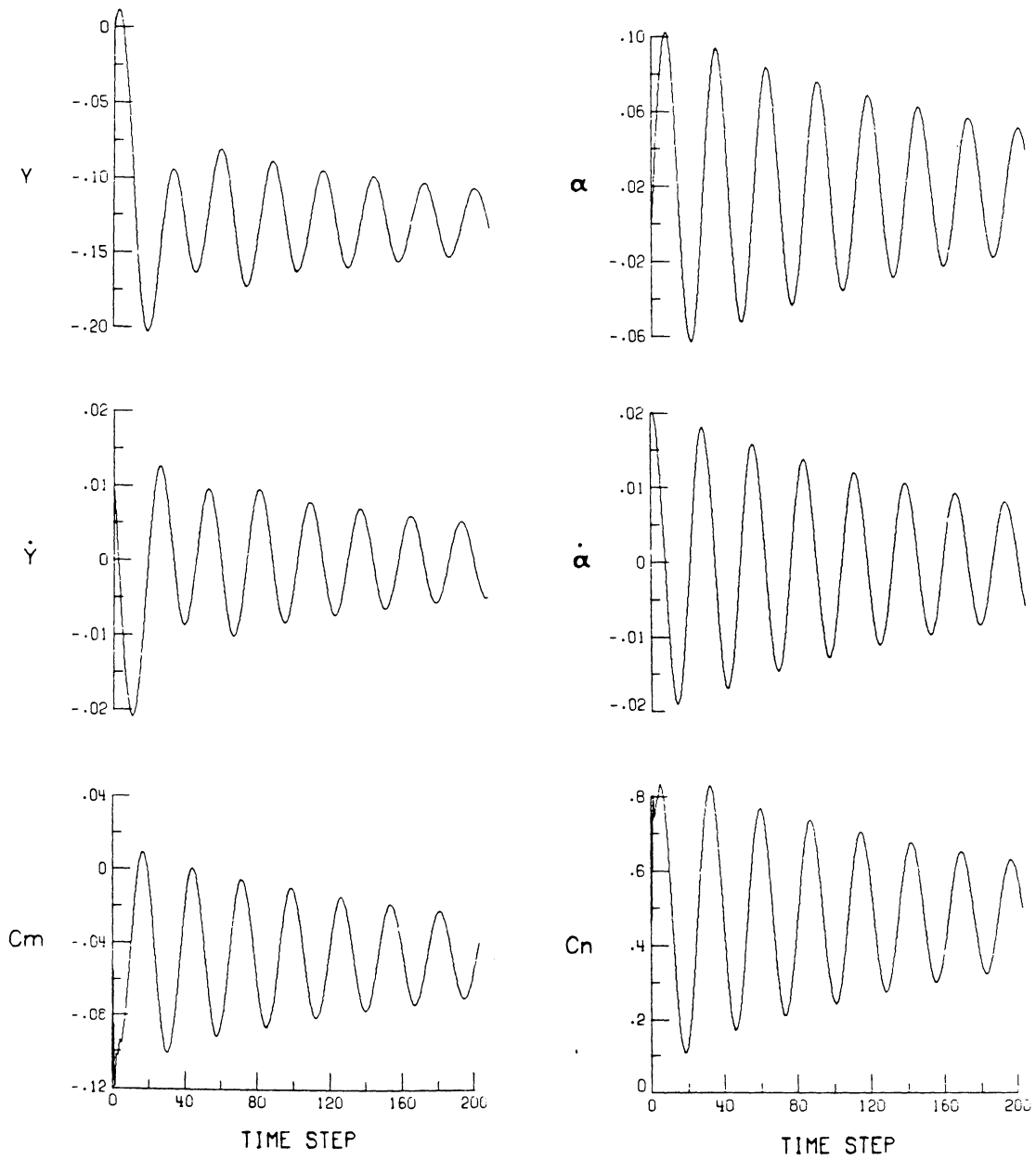
Figure 6.5. Response of the Rigid Wing at a Critical Dynamic
Pressure With Structural Damping Present.

nonlinearities; and (3) Fung's aerodynamic analysis is based upon two-dimensional, linear theory, and our method is based on the unsteady vortex-lattice concept.

6.3 An Example of Aeroelastic Behavior for the Elastic Wing

We now turn our attention to results predicted for example cases of our elastic-wing model. These results describe the responses to initial disturbances for dynamic pressures below and above the flutter boundary.

The physical properties of this elastic wing are given in Table 6.2. Although the structural model allows for the spanwise variation of all properties, we choose to demonstrate the procedure using a wing with constant sectional properties. The elastic axis is located at the sectional midchord, and the sectional center of mass is located aft of the elastic axis. The angle of attack is 15 degrees, this angle is defined as the angle of attack prior to the introduction of loading due to mass, steady aerodynamic loads, and unsteady aerodynamic loads.

The natural modes for the structure are required for the expansion of the dependent variables, w and α. This expansion is given in Chapter III. The Hunter method, described by Gray (1987), is used to determine the natural modes for the elastic wing. This method solves the two-point boundary value problem by a transfer matrix approach to the finite difference equations. Of course, the modes may be derived by any available computational or analytical method.

Table 6.2. Properties of the Elastic Wing Example

Wing aspect ratio	10.
Wing chord	1.0 ft
Bending stiffness	1.2×10^5 lb-ft^2
Torsional stiffness	7.0×10^4 lb-ft^2
Elastic axis/mass axis offset	.1 ft
Distributed mass	.537 lb-sec^2/ft^2
Distributed moment of inertia	.125 lb-sec^2

In this example we use the first and second bending modes and the first torsion mode to represent the deformations of the elastic axis of the wing. The normalized amplitudes of the mode shapes are tabulated in Table 6.3. The natural frequencies, scaled to the fundamental frequency in bending, are 1, 5.91, and 4.55.

As discussed in Chapter V, the solution to the equations for the elastic wing consist of both the static and dynamic solutions. Initially, an undeformed wing is placed in a steady flow. The deformations due to the static loads and weight are computed. If conditions are such that the wing will aeroelastically diverge, this will be determined during the computation of the static deformations. The dynamic response will be computed about the statically deformed shape.

6.3.1 Subcritical response of the elastic wing

In Figure 6.6, we show the response of the elastic wing when the dynamic pressure is below the critical dynamic pressure. The initial disturbance has the following form:

$$
\begin{array}{lll}
q_1 = 2.5 & q_2 = .25 & q_3 = .05 \\
\dot{q}_1 = 0.0 & \dot{q}_2 = 0.0 & \dot{q}_3 = 0.0
\end{array}
\tag{6.3}
$$

The generalized coordinates q_1 and q_2 are associated with the first two bending modes, q_3 is associated with the first torsion mode. These generalized coordinates are the time dependent coefficients in the expansions for the dependent variables. These coefficients give the dynamic contribution only.

Table 6.3. Natural Modes Used to Represent the Elastic Wing

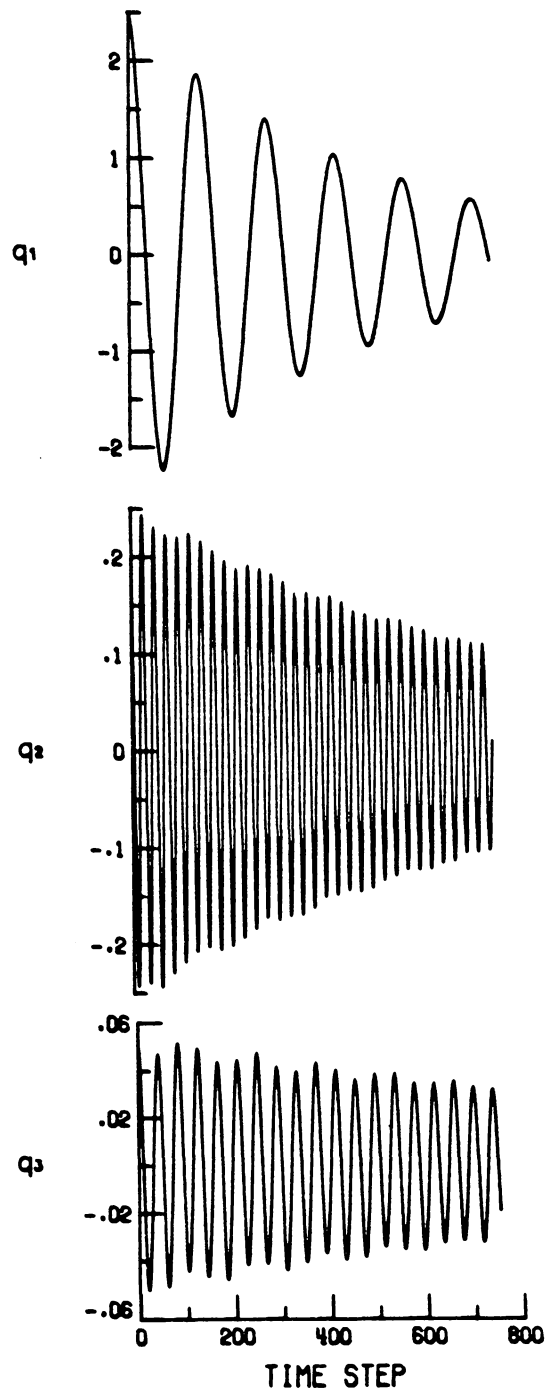| Station (% wing)	Bending First Mode (ω_{b_1} = .044*)	Bending Second Mode (ω_{b_2} = .260*)	Torsion First Mode (ω_{t_1} = .198*)
0. (root)	0.	0.	0.
.1	.0174	-.0978	.1563
.2	.0650	-.3001	.3088
.3	.1380	-.5169	.4538
.4	.2316	-.6687	.5875
.5	.3413	-.6975	.7068
.6	.4630	-.5753	.8088
.7	.5926	-.3064	.8908
.8	.7269	.0776	.9509
.9	.8632	.5287	.9876
1.0 (tip)	1.0	1.0	1.0

*Frequencies in radians/nondimensional time.

Figure 6.6. Response of the Elastic Wing at a Subcritical
Dynamic Pressure.

The motion decays for all three generalized coordinates to the statically deformed shape. In addition, the frequency of oscillation associated with the history of the generalized coordinates occurs at the natural, uncoupled frequency associated with each respective mode.

6.3.2 Critical response of the elastic wing

We now increase the dynamic pressure to that which creates the aeroelastic instability. This dynamic pressure was estimated by a method which will be discussed later. The initial disturbance has the following form:

$$q_1 = .25 \qquad q_2 = 0.0 \qquad q_3 = 0.0$$
$$\dot{q}_1 = 0.0 \qquad \dot{q}_2 = 0.0 \qquad \dot{q}_3 = 0.0 \qquad (6.4)$$

These initial conditions are smaller than those used for the subcritical case. The motion predicted by the simulations for the critical case, which use the initial disturbance expressed in Equation (6.3), grew excessively fast due to the large initial deformations. Hence, smaller disturbances are used and reflect the same instability but at a lower initial rate of growth.

In Figure 6.7 the response of the wing is represented by the time histories of the generalized coordinates. These coordinates are defined as in the previous case. The motion associated with the first bending mode (q_1) decays initially; however, after this initial period the motion appears to neither grow nor decay. Several harmonics (from the different modes) are embedded in this motion. The motion associated with the first torsion mode grows in time. The frequency of oscillation for this mode is near the fundamental torsional frequency.
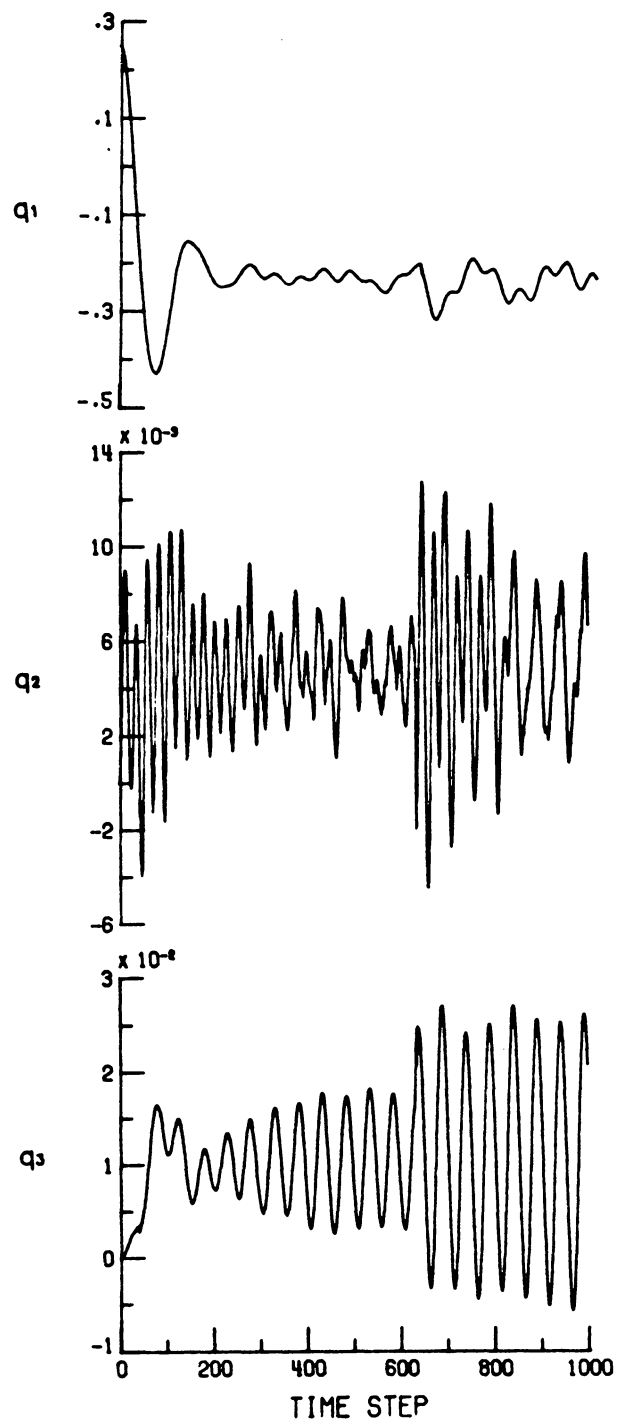
Figure 6.7. Response of the Elastic Wing at a Critical Dynamic Pressure.

The history of q_2 reflects the coupling necessary for flutter. Initially, the motion decays at the frequency associated with the second bending mode. Then, a shift in frequency and other harmonics appear. Around time step 600 one sees that the response (for all three coefficients) grows in amplitude. Finally, the frequency of the second mode coefficient coalesces with the torsional frequency. A flutter mode is created. The motion oscillates about a non-zero mean close to (but not coincident with) the static deflection. This drift is a nonlinear phenomenon (see Chapter 4 of the text by Nayfeh and Mook (1985)).

6.3.3 Supercritical response of the elastic wing

In the preceding case we considered a dynamic pressure very slightly above the critical dynamic pressure. We now increase the dynamic pressure to a larger value. The initial conditions are the same as those described by Equation (6.4).

The response of the wing to these conditions is shown in Figure 6.8. An interesting feature is contained in the predicted response of the torsion coefficient, q_3. The torsional contribution continues to grow. In fact, the oscillation grows to angles that would certainly cause the flow to separate from the surface, violating the assumptions used in the UVLM. However, more important is the fact that the motion is continually growing. Most likely, this motion would be catastrophic to the structure.

As a footnote, if we were to continue to increase the dynamic pressure it is possible that we could return to an aeroelastically
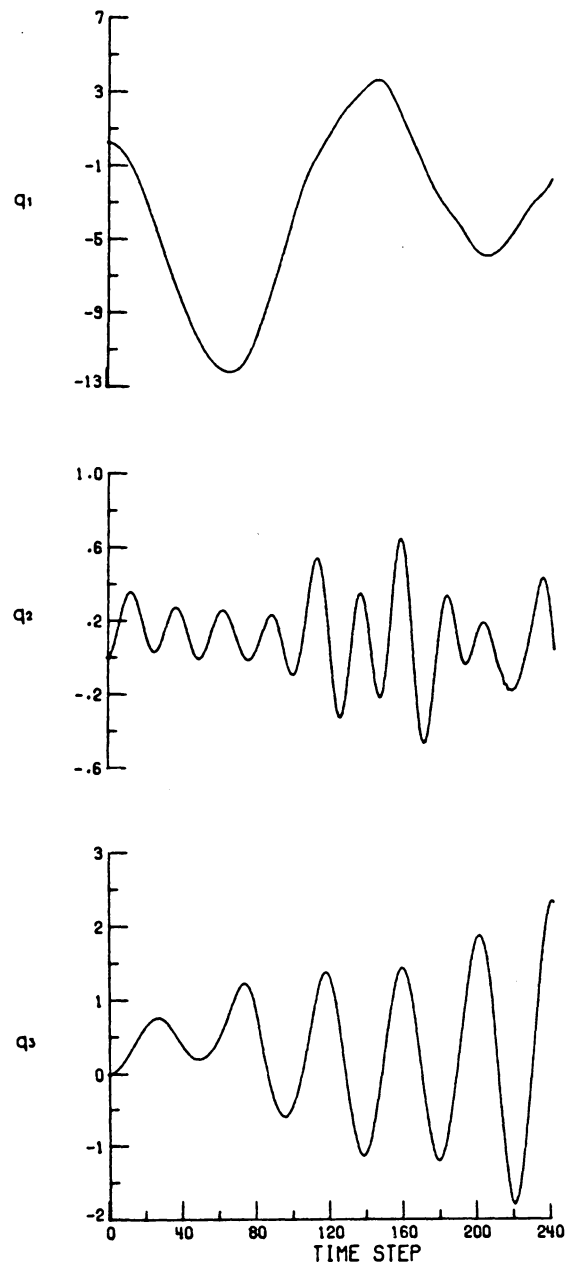
Figure 6.8. Response of the Elastic Wing at a Supercritical
Dynamic Pressure.

stable regime. This characteristic is illustrated in Figure 1.3. As the freestream speed is increased, one or more modes may cross into the unstable regime. These modes may return to the stable regime (as does the mode 3 root) and the structure is again stable. For obvious reasons, the lowest critical condition is of interest in aircraft or wind-tunnel model design.

6.3.4 Comparison with empirical results

Harris et al. (1963) described a method to approximate the flutter speed based upon empirical data. The method uses a baseline flutter speed index adjusted according to particular characteristics (e.g. aspect ratio, mass ratio, sweep angle, mass distribution, etc.) of the configuration under study. These adjustments are based upon parametric analyses of experimental and analytical studies.

For the elastic wing, the results reflect a constant freestream velocity which keeps the reduced (nondimensional) frequency nearly constant for all cases. The density of the fluid is modified which, in turn, modifies the dynamic pressure.

Using the approach described by Harris, the density required for the system to become unstable is approximately 0.026 slugs per cubic foot. In our calculations, a density of 0.0066 slugs per cubic foot was used for the stable (subcritical) case, a density of 0.035 slugs per cubic foot for the unstable (supercritical) case, and a density of 0.030 slugs per cubic foot for the marginally unstable (critical) case. There is very close agreement between the empirical and numerically simulated condition for marginal stability.

6.3.5 Unsteady aerodynamic loads

The aerodynamic loads and the motion of the wing are computed simultaneously and interactively. The primary objective of the numerical simulation is to determine the response of the wing and, in particular, determine whether or not the wing is aeroelastically stable. However, as a consequence, the unsteady aerodynamic loads are computed and the history of the pressure distribution on the wing could be used to describe the physics of aeroelastic response. Further, the technique could be modified by removing the structural model and restricting the wing motion to specified manuevers.

In Figure 6.9 we show the pressure distribution of the wing at three different times during the wing motion. The spanwise pressure distributions are shown for several chordwise stations. The values of the pressure differences are for the control points of the wing; the control points along the wing tips, leading edge, and trailing edge are not located directly on the edges of the wing.

In the upper portion the pressure distribution is shown for the wing due to static aerodynamic loads and the resulting static deformations. The pressure does decay toward the wing tips; however, a slight rise in pressure is indicated near these edges as a result of wing-tip vortices. The effect of the second bending mode is clearly evident. The pressure distribution along the chord (for a constant spanwise station) reflects that distribution one would expect from classical theory; the peak pressures are at the leading edge and these pressures decay to a near-zero value at the trailing edge as dictated by the Kutta condition. The pressure distribution is also shown at
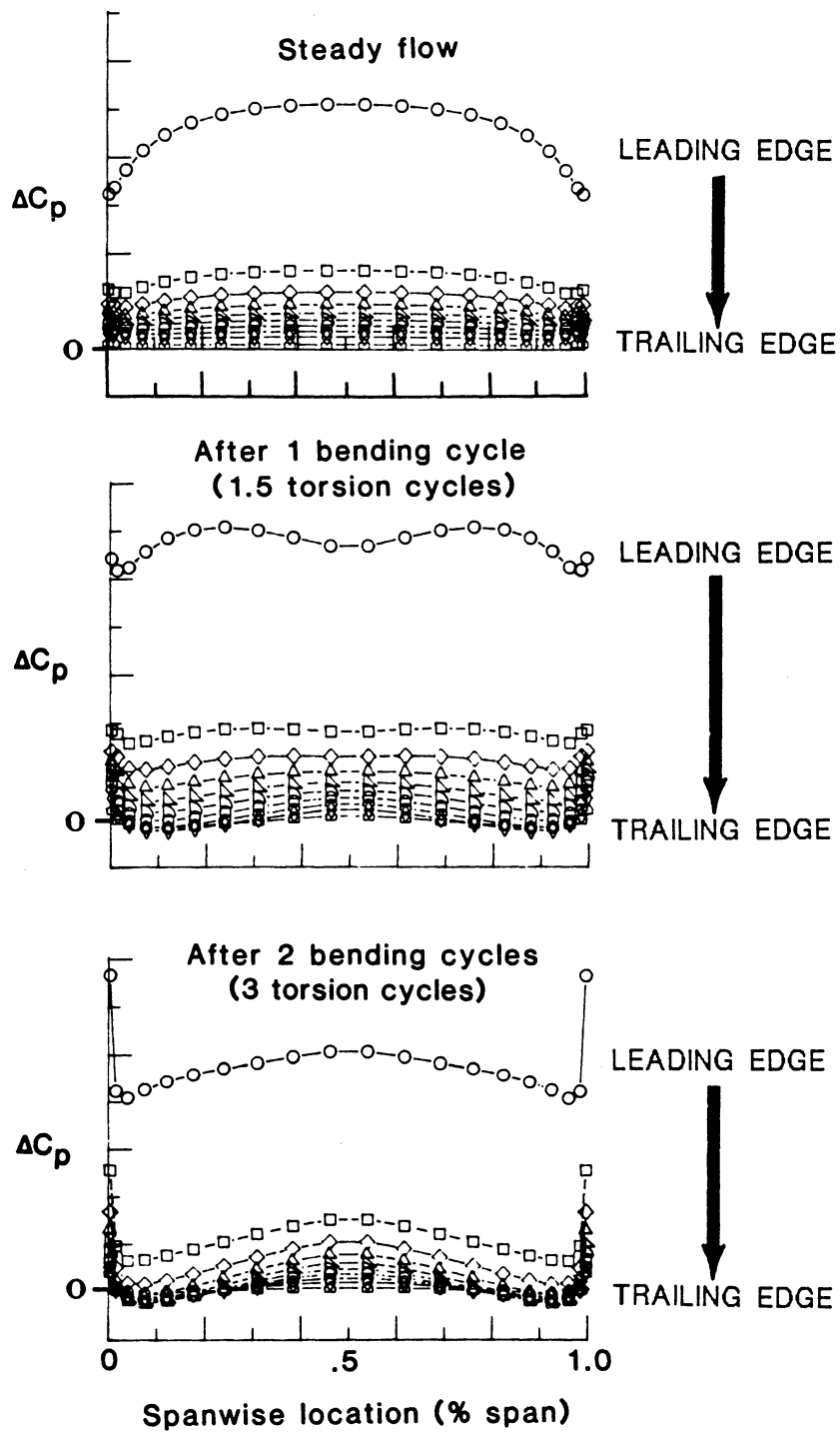
Figure 6.9. The Pressure Distribution of the Elastic Wing
at Three Different Times.

two times during the motion of the wing. Again, the effect of the
second bending mode is clearly evident. The effect of the strong
wing-tip vortex systems created by the rapid motion is particularly
evident in the bottom part of the figure.

In Figure 6.10 the (nondimensional) time history of the pressure
distribution for individual elements is traced. We show the pressure
difference across four elements: the wing-tip leading-edge, the wing-
tip trailing-edge, the wing-root leading-edge, and the wing-root
trailing-edge elements. The wing-tip elements experience large-
amplitude motions; hence, large fluctuations occur. In contrast, the
wing-root elements do not experience large motion because of the
fixed-wing boundary condition; hence, smaller fluctuations occur. The
pressure differences for the two trailing-edge elements are near zero
which substantiates the presence of the Kutta condition in our
aerodynamic model.

In Figure 6.11 the (nondimensional) time histories of the aero-
dynamic normal-force and pitching-moment coefficients are shown for
the wing-root, mid-span, and wing-tip locations. These coefficients
are computed from the pressure distributions associated with the
column of lattice elements located at these spanwise stations. As one
would expect, the coefficients oscillate at frequencies associated
with the natural modes. The peaks do not occur at the same time at
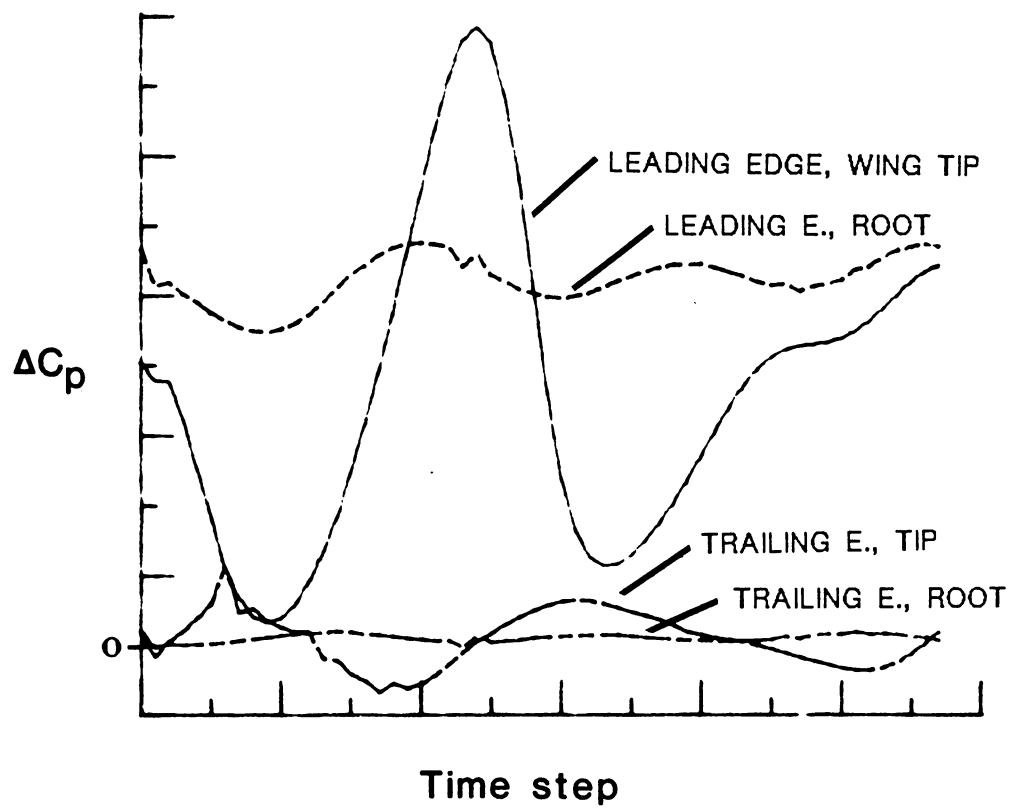all stations.

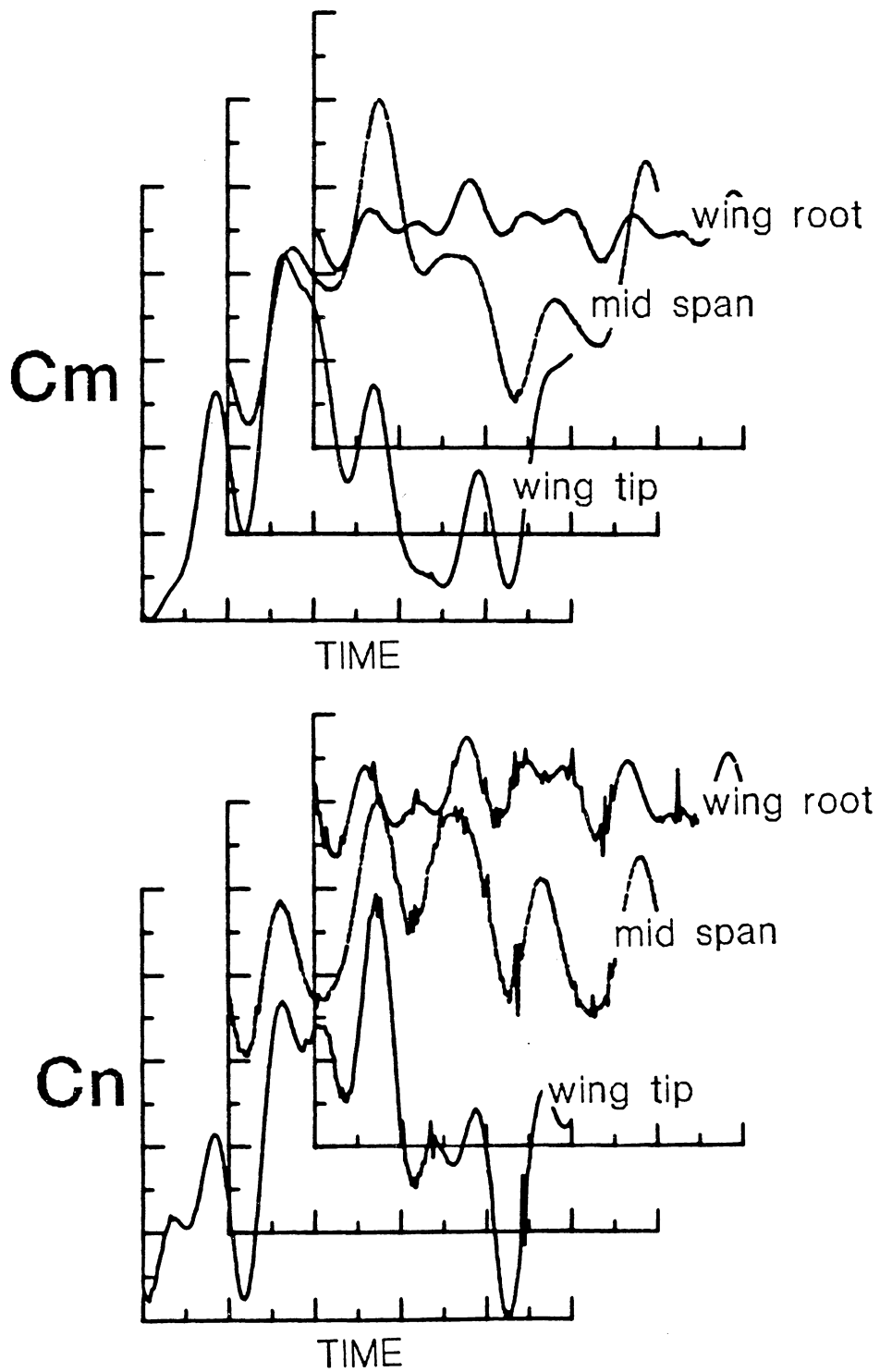Figure 6.10. The Predicted Pressure Distribution for
Four Selected Elements.

Figure 6.11. Sectional Aerodynamic Coefficients Predicted by the Model.

6.4 The Identification of Flutter

We have shown the response of the rigid wing and the elastic
wing to conditions which result in both aeroelastic stability and
instability. However, the technique which determines the precise dy-
namic pressure necessary for the instability has not been discussed.
Although not within the scope of this research, ultimately we are in-
terested in determining the lowest possible dynamic pressure at which
initial disturbances will not decay. Once this exact condition can be
ascertained then the effects of angle of attack, aspect ratio, or
other nonlinearities may be examined.

Currently, we increase the freestream conditions (dynamic pres-
sure) from a known stable position, simulate the response of the wing
to an initial disturbance, and examine the response of the wing. At
some point it is clear that the motion is growing and that a flutter
mode exists. However, we have only bounded the critical dynamic pres-
sure. It is difficult to determine the precise dynamic pressure at
which the wing becomes unstable. In some cases, the motion associated
with a degree (or degrees) of freedom appears to grow while the motion
for another degree (or degrees) of freedom appears to decay. In
addition, several simulations are required. A method is needed to
identify this critical point with a minimum of required simulations.

The frequency domain solutions (Desmarais et al., 1978) determine
this critical point by tracking the eigenvalues (and associated aero-
dynamic damping) of the system for increasing velocities. We briefly
describe these methods in Chapter I, the reader is referred to Fig-
ure 1.3. Hassig (1971) demonstrated a similar approach by examining

the damping associated with the assumed harmonic motion. Time domain solutions (Dowell et al., 1980) typically use logarithmic decrement approaches to determine the flutter boundary. However, these methods assume a form of the solution.

A method to determine the exact flutter boundary as predicted by the numerical simulation has not been fully developed; however, two promising approaches have been initiated. The first approach is based on a parametric identification procedure which is described by Konstadinopoulos (1984) and Elzebda (1986). The second approach is based on an energy method. The approaches will be briefly described.

6.4.1 Parametric identification procedures

Adopting the approach described by Konstadinopoulos, one can model the nonlinear motion of the wing by assuming the normal-force and pitch-moment coefficients are nonlinear functions of α, $\dot{Y}$, and $\dot{\alpha}$. An equation for each aerodynamic coefficient is formed which contains the higher-order terms. A quintic nonlinearity is suspected; therefore, the equations contain all 55 terms up to and including the fifth-order terms.

The aerodynamic normal-force coefficient is represented by the following equation:

$$C_n = a_1\dot{Y} + a_2\alpha + a_3\dot{\alpha} + a_4\dot{Y}^2 + a_5\alpha^2 + a_6\dot{\alpha}^2 + \ldots$$

$$+ a_{54}\dot{Y}^2\alpha\dot{\alpha}^2 + a_{55}\dot{Y}\alpha^2\dot{\alpha}^2 + \text{h.o.t.} \tag{6.5}$$

The aerodynamic pitching-moment coefficient is represented by the following equation:

$$C_m = b_1 \dot{Y} + b_2 \alpha + b_3 \dot{\alpha} + b_4 \dot{Y}^2 + b_5 \alpha^2 + b_6 \dot{\alpha}^2 + \ldots$$

$$+ b_{54} \dot{Y}^2 \alpha \dot{\alpha}^2 + b_{55} \dot{Y} \alpha^2 \dot{\alpha}^2 + \text{h.o.t.} \tag{6.6}$$

We then fit the aerodynamic coefficient versus time curves - such as those curves shown in Figures 6.1, 6.2, and 6.3 - using a least-squares technique to determine the coefficients a_i and b_i. By taking off one term at a time we are able to identify those terms which have a negligible contribution. The remaining terms provide a simple expression for the aerodynamic coefficients.

The coefficients a_i and b_i will be unique for a particular dynamic pressure, static angle of attack, spring constant, etc. Konstadinopoulos classified the coefficients as either restoring terms or damping terms. By examining the value and, in particular, the sign change of the damping terms versus the critical parameter (the angle of attack), he was able to identify the angle of attack at which wing-rock occurs.

Our critical parameter is the dynamic pressure and we are interested in the minimum value at which initial disturbances do not decay. This parameter will be identified by extracting from the damping coefficient versus dynamic pressure curve the condition at which the sign for the damping changes.

Unfortunately, our results have not yielded the same success as the work of Konstadinopoulos. Several complications are introduced when the method is extended to the aeroelastic application. First, we are working with two aerodynamic coefficients. Second, the terms of the fifth-order equations (see Eqs. (6.5) and (6.6)) which are eliminated are a function of the dynamic pressure; hence, the form of the expression is not quite the same for all cases. Third, the use of the method for the elastic wing will certainly be complicated by the spanwise variation and phase relationships of the aerodynamic coefficients.

Yet, the concept of examining the character of the damping of the system is consistent with the frequency and time domain methods addressed in the literature. Therefore, the method may yet be the key in future determinations of the exact critical condition.

6.4.2 Identification using the system energy

An alternate method is suggested to determine the critical condition necessary for an instability. This method determines the total work being done on the system by the loads during the simulation. The method is based on the concept that an aeroelastic instability exists when more energy is being extracted from the freestream by the wing, then pumped back into it by the wing. Therefore, an instability is present when the total energy level of the wing grows in time.

In Chapter III we develop the equations of motion for the elastic wing. The kinetic energy of the wing is expressed by Equation (3.3)

and the potential energy of the wing is expressed by Equation (3.4). These equations are repeated here for convenience.

$$T = \int_0^L \frac{1}{2} \left[m(y)(\{\dot{w} + x_\alpha(y)(\cos\alpha)\dot{\alpha}\}^2 \right.$$

$$\left. + \{x_\alpha(y)(\sin\alpha)\dot{\alpha}\}^2) + I_{cg}(y)\dot{\alpha}^2 \right] dy \qquad (3.3)$$

$$V = \int_0^L \frac{1}{2} \left[EI(y)w''^2 + GJ(y)\alpha'^2 \right.$$

$$\left. - m(y)g[w + x_\alpha(y)\sin\alpha] \right] dy \qquad (3.4)$$

The total energy is the sum of the kinetic energy and the potential energy. The state variables which have previously been predicted through a simulation and describe the motion of the wing are substituted into the energy expressions.

Expressions that give the total energy for the rigid wing are available from the formulation of the equations of motion described in Chapter II. The method is illustrated through an example utilizing the rigid-wing model.

Figure 6.12 describes the time history of the wing in motion for both a stable and an unstable case. The predicted motion of the wing $(Y,\dot{Y},\alpha,\dot{\alpha})$ is used in the expression for the total energy. The stable case is characterized by an oscillating, yet decaying, level of energy and will reach a constant energy level associated with the steady-state (i.e. static) conditions. The unstable case is characterized by an oscillating, yet growing, level of energy. If the dynamic pressure
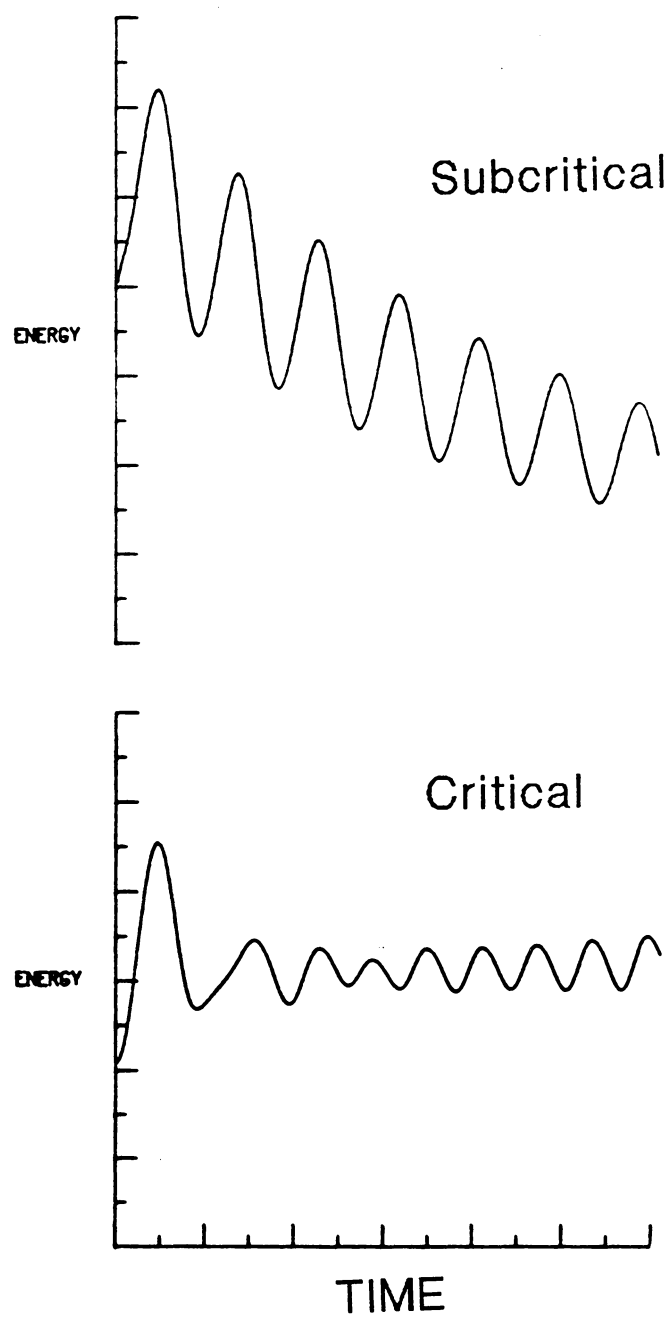
Figure 6.12.   The Computed Energy of the Rigid Wing for a
Subcritical and Critical Case.

is slightly above the critical condition then the motion may be governed by system nonlinearities and the total energy level will fluctuate around a nonzero mean.

The advantage of the method is that now, instead of examining the motion associated with each degree of freedom or fitting the aerodynamic coefficients with high-order polynomials, a single quantity is used. The method applies to both the elastic wing and the rigid wing models.

The disadvantage is that a transition from the stable to the unstable case is still difficult to ascertain. One possible method is to measure the decrement associated with the decaying oscillation and extract a damping term from the energy curve. Negative damping indicates the instability.

6.5 Wing and Wake Graphics

An advantage of the general technique is that the time domain solution coupled with the UVLM provides the capability of graphically depicting wing and wake motion. Now, the physics of aeroelastic response can be graphically described.

We have previously demonstrated the capability (Chapter IV) of generating graphical representations of the flowfield. We now address the generation of movies of the wing and wake motion as predicted by the general model. Recently, we (Strganac and Mook (1987), and Strganac, Mook, and Mitchum (1987)) presented movies of the wing and wake motion. Both stable and unstable behaviors of the wing were shown.

In Figure 6.13 we show the vorticity for the wing at several time steps. The frames are extracted from the movie. The view is from above the wing surface. Near the top of each frame is the leading edge of the wing. The brighter regions, typically those regions near the leading edge, indicate the more intense concentrations of vorticity. As the wing twists and bends in response to the initial condition, the vorticity on the wing changes. It is important to reiterate that, in turn, the motion is also a function of this vorticity through the unsteady aerodynamic loads.

In Figure 6.14 we show the vorticity and shape of the wing and wake at several time steps (which correspond to Fig. 6.13). The history of the previous motion is embedded in the wake. The character of the vorticity is also indicative of the current motion of the wing. The motion of the wing can also be seen in the sequence.

For purposes of illustration, the physical properties of the system are such that for every three cycles of (first mode) bending motion there are two cycles of (first mode) torsion motion. The geometry of the wing and wake continues to change. It is interesting to note that the wing-tip vortex system breaks down and reforms with the bending/torsion motion. The aerodynamic loads which are used to calculate the motion reflect this behavior.

STEADY STATE

10th Time Step

20th Time Step

30th Time Step

40th Time Step

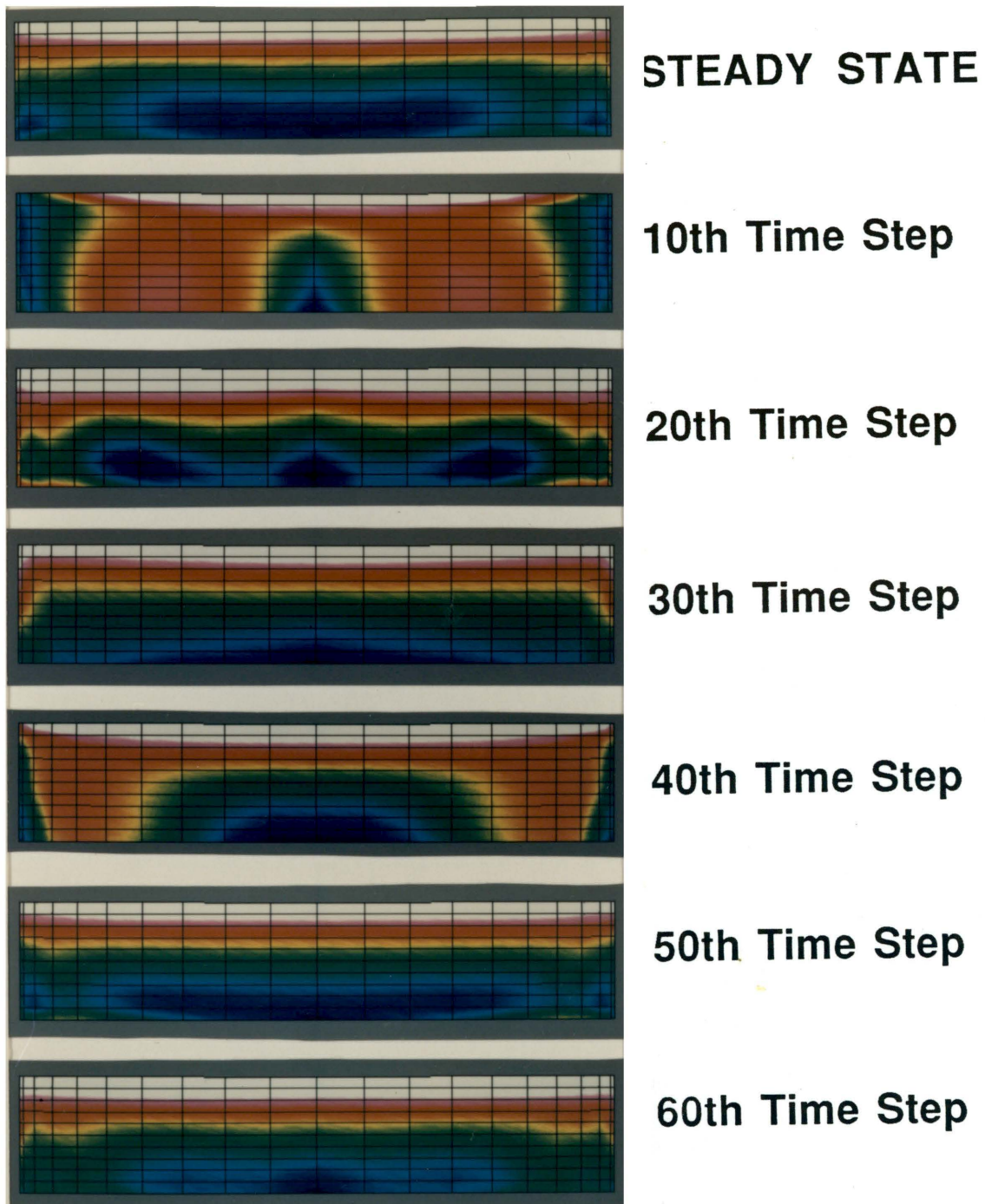**50th Time Step**

60th Time Step

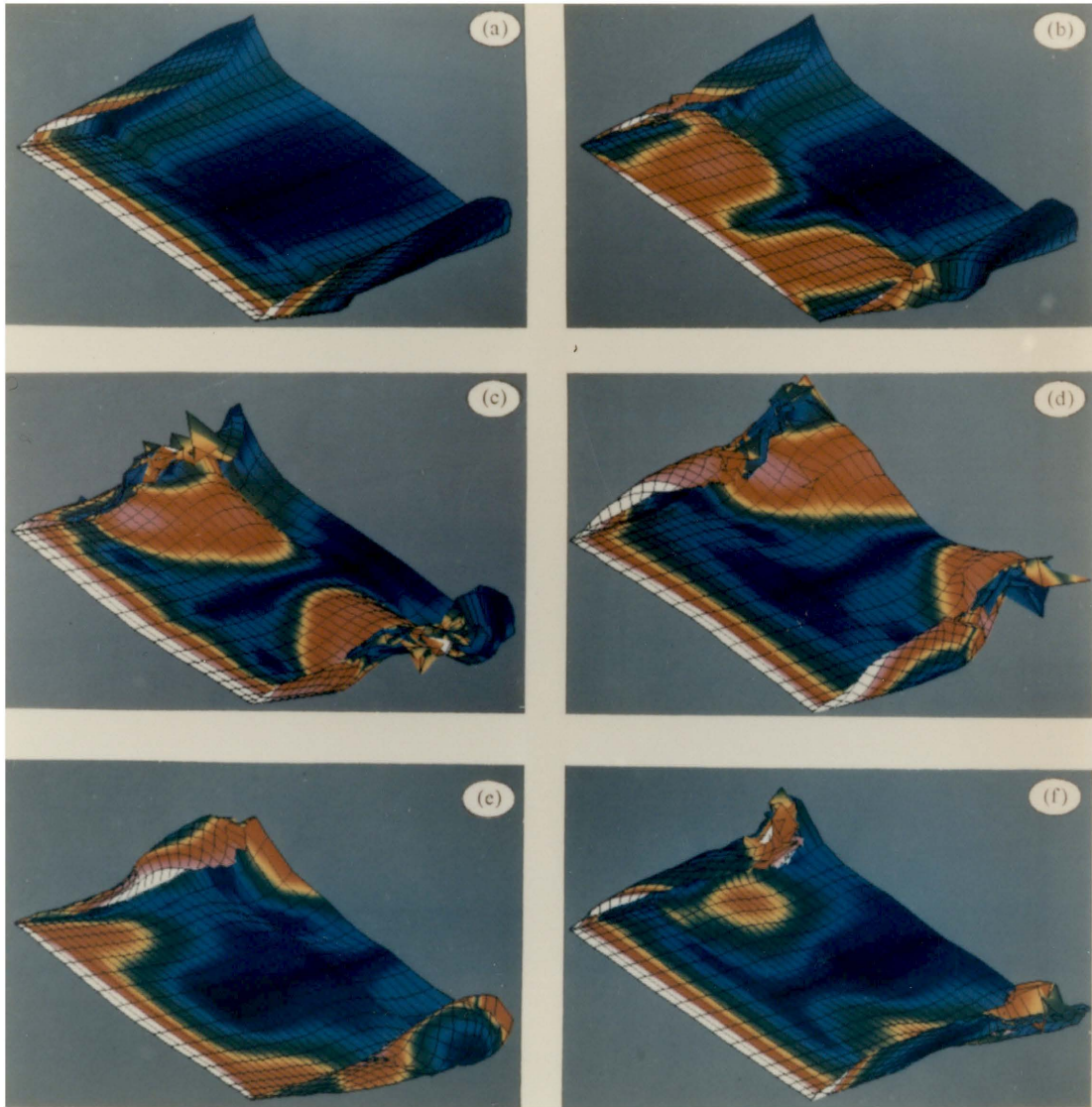Figure 6.13. The Strength of Vorticity for the Wing at
Several Time Steps.

Figure 6.14.   The Predicted Shape and Strength of Vorticity
for the Wing and Wake at Several Time Steps.

CHAPTER VII

CONCLUDING REMARKS

A numerical model has been described that predicts the steady and unsteady aeroelastic behavior of a wing. The method can predict steady-state static responses and transient responses to initial disturbances. The solution of the governing equations is obtained in the time domain. A physical interpretation of the response is aided by animation of the wing and flowfield histories.

An aerodynamic model is introduced into the formulation which addresses nonlinearities created by static deformations, angles of attack, vorticity dominated flows, and unsteady flowfields. The wake is computed as part of the solution; hence, the history of the motion is included in the technique. Steady and unsteady aerodynamic loads are also computed as part of the solution.

The numerical model has been developed such that the aerodynamic and structural models may be independently modified. As a result, nonlinear structural models or other aerodynamic models may be introduced in the future. Two structural models are demonstrated: the rigid wing mounted to a linear elastic support and the elastic wing cantilevered from a rigid support. Both formulations treat the nonlinear effects of static angle of attack and displacements.

The equations governing the motion of the structure are coupled with the equations governing the motion of the fluid, and the structure and fluid are treated as a single dynamical system. The integration of the governing equations using the predictor-corrector technique requires convergence of the loads and motion at each time step of integration.

REFERENCES

Ashley, H., Lehman, L. L., and Nathman, J. K., The Constructive Uses of Aeroelasticity, AIAA Paper No. 80-0877, AIAA International Annual Meeting and Technical Display, 1980.

Atta, E. H., Unsteady Flow Over Arbitrary Wing Planforms Including Tip Separation, M.S. Thesis, Department of Engineering Science and Mechanics, Virginia Polytechnic Institute and State University, Polytechnic, 1976.

Atta, E. H., Kandil, O. A., Mook, D. T., and Nayfeh, A. H., Unsteady Flow Past Wings Having Sharp-Edge Separation, NASA SP-405, 1976.

Atta, E. H., Kandil, O. A., Mook, D. T., and Nayfeh, A. H., University Aerodynamic Loads on Arbitrary Wings Including Wing-Tip and Leading Edge Separation, AIAA Paper No. 77-156, 1977.

Atta, E. H., Nonlinear Steady and Unsteady Aerodynamics of Wings and Wing-Body Combinations, Ph.D. Dissertation, Department of Engineering Science and Mechnics, Virginia Polytechnic Institute and State University, 1978.

Batina, J. T., Seidel, D. A., Bland, S. R., and Bennett, R. M., Unsteady Transonic Flow Calculations for Realistic Aircraft Configurations, AIAA Paper Number 87-0850, 28th Structures, Structural Dynamics, and Materials Conference, April 6-8, 1987.

Belotserkovskiy, S. M., Calculating the Effects of Gusts on an Arbitrary Thin Wing, Fluid Dynamics, Volume 1, No. 1, 1966.

Belotserkovskiy, S. M., Calculation of the Flow around Wings of

Arbitrary Planform in a Wide Range of Angles of Attack, NASA TT

F-12,291, May 1968.

Belotserkovskiy, S. M. and Nisht, M. I., Nonstationary Nonlinear

Theory of a Thin Wing of Arbitrary Planform, Fluid Dynamics,

Volume 9, No. 4, 1974.

Bendiksen, O. O. and White, J. F. III, Aeroelastic Tailoring of

Advanced Composite Compressor Blades, AIAA Paper No. 86-1008,

1986.

Biot, M. A. and Arnold, L., Low-Speed Flutter and Its Physical

Interpretation, Journal of the Aeronautical Sciences, Volume 15,

No. 4, April 1948.

Bisplinghoff, R. L., Ashley, H., and Halfman, R. L., Aeroelasticity,

Addison-Wesley Publishing Company, Inc., Reading, Massachusetts,

1955.

Bisplinghoff, R. L. and Ashley, H., Principles of Aeroelasticity,

Dover Publications, Inc., New York, 1975.

Carnahan, B., Luther, H. A., and Wilkes, J. O., Applied Numerical

Methods, John Wiley & Sons, Inc., New York, 1969.

Collar, A. R., The First Fifty Years of Aeroelasticity, Aerospace,

February 1978.

Crespo da Silva, M. R. M. and Hodges, D. H., Nonlinear Flexure and

Torsion of Rotating Beams, with Application to Helicopter Rotor

Blades - I. Formulation, and - II. Response and Stability

Results, Vertica, Volume 10, No. 2, 1986.

Desmarais, R. N. and Bennett, R. M., User's Guide for a Modular Flutter Analysis Softwear System (FAST Version 1.0), NASA TM 78720, 1978.

Devers, A. D., A General Method for Calculating Three Dimensional Nonstationary Aeroelastic Response in Subsonic Flows, Arnold Engineering Development Center TR-72-59, May 1972.

Dowell, E. H. (Editor), et al., A Modern Course in Aeroelasticity, Sijtohoff & Noordhoff International Publishers, Alphen ann den Rijn, The Netherlands, 1980.

Edwards, J. W., Applications of Potential Theory Computations to Transonic Aeroelasticity, ICAS-86 - 2-9.1, 1986.

Elzebda, J. M., Mook, D. T., and Nayfeh, A. H., Unsteady Aerodynamic Interference for Lifting Surfaces, AIAA Paper Number 85-1801, 1985.

Elzebda, J. M., Two-Degree-of-Freedom Wing Rock and Nonlinear Aerodynamic Interference, Ph.D. Dissertation, Department of Engineering Science and Mechanics, Virginia Polytechnic Institute and State University, December 1986.

Farmer, M. G., A Two-Degree-of-Freedom Mount System with Low Damping for Testing Rigid Wings at Different Angles of Attack. NASA TM 83302, 1982.

Franz, H. P., Krenz, G., and Kotschote, J., Load-Depending Deformations of Windtunnel Models, AIAA Paper No. 84-0589, AIAA 13th Aerodynamic Testing Conference, March 5-7, 1984.

Fung, Y. C., An Introduction to the Theory of Aeroelasticity, John Wiley & Sons, Inc., New York 1955.

Garrick, I. E., Aerodynamic Flutter, Volume V, AIAA Selected Reprint Series, March 1969.

Goland, M. and Luke, Y. L., A Study of the Bending-Torsion Aeroelastic Modes for Aircraft Wings, Journal of the Aeronautical Sciences, Volume 16, Number 7, July 1949.

Gray, C. E. Jr., Coupled Bending - Torsion Steady-State Response of Pretwisted, Nonuniform Rotating Beams Using a Transfer-Matrix Method, M.S. Thesis, Old Dominion University, 1987.

Hancock, G. J., Wright, J. R., and Simpson, A., On the Teaching of the Principles of Wing Flexure-Torsion Flutter, Aeronautical Journal, October 1985.

Harris, G., Head, A. L. Jr., and Starr, G. A., Flutter Criteria for Preliminary Design, DDC No. AD-346962, 1963.

Hassig, H. J., An Approximate True Damping Solution of the Flutter Equation by Determinant Iteration, AIAA Journal of Aircraft, Volume 8, No. 11, Nov. 1971.

Hodges, D. H. and Dowell, E. H., Nonlinear Equations of Motion for the Elastic Bending and Torsion of Twisted Nonuniform Rotor Blades, NASA TN D-7818, 1974.

Hsu, P. T., Some Recent Developments in the Flutter Analysis of Low-Aspect-Ratio Wings, Department of the Navy Contract No. NOa 55-771-c, 1957.

James, R. M., On the Remarkable Accuracy of the Vortex Lattice Method, Computer Methods in Applied Mechanics and Engineering 1, 1972.

Kandil, O. A., Mook, D. T., and Nayfeh, A. H., Nonlinear Prediction of
the Aerodynamic Loads on Lifting Surfaces, AIAA Paper Number
74-503, 1974.

Kandil, O. A., Prediction of the Steady Aerodynamic Loads on Lifting
Surfaces Having Sharp-Edge Separation, Ph.D. Dissertation,
Department of Engineering Science and Mechanics, Virginia
Polytechnic Institute and State University, 1974.

Kandil, O. A., Mook, D. T., and Nayfeh, A. H., New Convergence Crite-
ria for the Vortex-Lattice Models of the Leading-Edge Separation,
NASA SP-405, 1976.

Kandil, O. A., Atta, E. H., and Nayfeh, A. H., Three Dimensional
Steady and Unsteady Asymmetric Flow Past Wings of Arbitrary Plan-
forms, AGARD Paper No. 2, AGARD Fluid Dynamics Panel Symposium,
Unsteady Aerodynamics, Ottawa, Canada, 1977.

Karamcheti, K., Principles of Ideal-Fluid Aerodynamics, Robert E.
Krieger Publishing Company, Inc., Malabar, Florida, 1980.

Kaza, K. R. V. and Kvaternik, R. G., Nonlinear Aeroelastic Equations
for Combined Flapwise Bending, Chordwise Bending, Torsion, and
Extension of Twisted Nonuniform Rotor Blades in Forward Flight,
NASA TM-74059, August 1977.

Kobayakawa, M. and Onuma, H., Propeller Aerodynamic Performance by
Vortex-Lattice Method, Journal of Aircraft, Volume 22, No. 8,
1985.

Konstadinopoulos, P., A Vortex-Lattice Method for General, Unsteady,
Subsonic, Aerodynamics, M.S. Thesis, Virginia Polytechnic
Institute and State University, July 1981.

Konstadinopoulos, P., Mook, D. T., and Nayfeh, A. H., A Numerical Method for General Unsteady Aerodynamics, AIAA Paper Number 81-1877, AIAA Atmospheric Flight Mechanics Conference, August 1981.

Konstadinopoulos, P., Numerical Simulation of the Subsonic Wing-Rock Phenomenon, Ph.D. Dissertation, Department of Engineering Science and Mechanics, Virginia Polytechnic Institute and State University, March 1984.

Konstadinopoulos, P., Thrasher, D. F., Mook, D. T., Nayfeh, A. H., and Watson, L., A Vortex-Lattice Method for General, Unsteady Aerodynamics, Journal of Aircraft, Volume 22, Number 1, January 1985.

Konstadinopoulos, P., Mook, D. T., and Nayfeh, A. H., Subsonic Wing Rock of Slender Delta Wings, Journal of Aircraft, Volume 22, March 1985.

Loring, S. J., General Approach to the Flutter Problem, Society of Automotive Engineers Journal, August 1941.

Maddox, S. A., An Extension of Vortex-Lattice Method to Include the Effects of Leading-Edge Separation, M.S. Thesis, Virginia Polytechnic Institute and State University, 1973.

Meirovitch, L., Computational Methods in Structural Dynamics, Sitjthoff & Noordhoff International Publishers, Alphen aan den Rijn, The Netherlands, 1980.

Mook, D. T. and Nayfeh, A. H., Application of the Vortex-Lattice Method to High-Angle-of-Attack Subsonic Aerodynamics, SAE Technical Paper Series 851617, 1985.

Mook, D. T. and Maddox, S. A., An Extension of a Vortex-Lattice Method to Include the Effects of Leading-Edge Separation, Journal of Aircraft, Volume 11, No. 2, 1974.

Nayfeh, A. H. and Mook, D. T., Nonlinear Oscillations, John Wiley & Sons, Inc., New York, 1979.

Nayfeh, A. H., Mook, D. T., and Yen, A., The Aerodynamics of Small Harmonic Oscillations around Large Angles of Attack, AIAA Paper No. 79-1520, 1979.

Pines, S., An Elementary Explanation of the Flutter Mechanism, Proceedings of the National Specialists Meeting on Dynamics and Aeroelasticity, November 1958.

Rivello, R. M., Theory and Analysis of Flight Structures, McGraw-Hill Book Company, New York, 1969.

Strganac, T. W. and Mook, D. T., The Application of the Unsteady Vortex Lattice Method to the Nonlinear Two Degree-of-Freedom Aeroelastic Equations, AIAA Paper No. 86-0867, 27th Structures, Structural Dynamics, and Materials Conference, May 19-21, 1986.

Strganac, T. W. and Mook, D. T., A New Method to Predict Unsteady Aeroelastic Behavior, AIAA Paper Number 87-0736, 28th Structures, Structural Dynamics, and Materials Conference, April 6-8, 1987.

Strganac, T. W., Mook, D. T., and Mitchum, M. V., The Numerical Simulation of Subsonic Flutter, AIAA Paper Number 87-1428, 19th Fluid Dynamics Conference, June 1987.

Theodorsen, T., General Theory of Aerodynamic Instability and the Mechanism of Flutter, NACA Report No. 496, 1940.

Thomas, J. L. and Nerney, B., Aerodynamics of Arbitrary Wing Body
    Combinations with Vortex Lattice and Slender Body Theory, AIAA
    Paper No. 76-198, AIAA 14th Aerospace Sciences Meeting, January
    26-28, 1976.

Thrasher, D. F., Mook, D. T., Kandil, O. A., and Nayfeh, A. H.,
    Application of the Vortex-Lattice Concept to General, Unsteady
    Lifting - Surface Problems, AIAA Paper No. 77-1157, 1977.

Thrasher, D. F., Nonlinear Unsteady Aerodynamics with Application to
    Dynamic-Aerodynamic Interaction, M.S. Thesis, Department of
    Engineering Science and Mechanics, Virginia Polytechnic Institute
    and State University, 1979.

Weisshaar, T. A., Aeroelastic Tailoring - Creative Uses of Unusual
    Materials, AIAA Paper 87-0976-CP, 28th Structures, Structural
    Dynamics, and Materials Conference, 1987.

Yates, E. C., Jr. and Bennett, R. M., Analysis of Supersonic-
    Hypersonic Flutter of Lifting Surfaces at Angle of Attack.
    AIAA Paper No. 71-327, 12th Structures, Structural Dynamics,
    and Materials Conference, April 19-21, 1971.

Yates, E. C., Jr., Flutter and Unsteady-Lift Theory, Performance and
    Dynamics of Aerospace Vehicles, NASA SP-258, 1971.

Yates, E. C., Jr., Wynne, E. C., and Farmer, M. G., Measured and
    Calculated Effects of Angle of Attack on the Transonic Flutter of
    a Supercritical Wing, AIAA Paper No. 82-0647, 23rd Structures,
    Structural Dynamics, and Materials Conference, May 10-12, 1982.

Yates, E. C., Jr., Unsteady Subsonic and Supersonic Flows - Historical
    Review; State of the Art, Computational Methods in Potential
    Aerodynamics, Springer Verlag, 1985.